

Particle Transport in Large Networks

L. Lizana and Z. Konkoli

Department of Applied Physics, Chalmers University of Technology and Goteborg University
(Dated: May 23, 2019)

We developed analytical and numerical methods to study a transport of non-interacting particles in large networks consisting of M d -dimensional containers $C_1; \dots; C_M$ with radii R_i linked together by tubes of length l_{ij} and radii a_{ij} where $i, j = 1; 2; \dots; M$. Tubes may join directly with each other forming junctions. It is possible that some links are absent. Instead of solving the diffusion equation for the full problem we formulated an approach that is computationally more efficient. We derived a set of rate equations that govern the time dependence of the number of particles in each container $N_1(t); N_2(t); \dots; N_M(t)$. In such a way the complicated transport problem is reduced to a set of M first order integro-differential equations in time, which can be solved efficiently by the algorithm presented here. The rate equations are valid for any network topology under the assumption that the tubes are thin in comparison to their lengths and the radii of the containers, $a_{ij} \ll R_i; R_j; l_{ij}$. Under these assumptions the containers can be considered ideally mixed at all times and transport through the tubes is one-dimensional. These assumptions were verified numerically. The workings of the method have been demonstrated on a couple of examples: networks involving three, four and seven containers, and one network with a three-point junction. Already simple networks with relatively few containers exhibit interesting transport behavior. For example, we showed that it is possible to adjust the geometry of the networks so that the particle concentration varies in time in a wave-like manner. Such behavior deviates from simple exponential growth and decay occurring in the two container system. In addition, we showed how to eliminate junctions from the dynamical equations in the large time limit.

I. INTRODUCTION

Many processes in nature can be described in terms of abstract mathematical networks, defined as a set of nodes and links, and there are numerous examples that occur in many diverse fields [1]: national power grids, neural networks (neurons and synapses), social networks (people and contacts), the Internet (computers and routers), the World Wide Web (web pages and hyper links) and the living cell (reactants are identified as nodes and the connection between two nodes implies that the corresponding reactants participate in some reaction) [2].

In general, network studies can be separated into three categories. (i) The topology of the network can change in time where nodes and links may be added or taken away according to certain rules [1, 3, 4]. (ii) Networks can be used as a platform that sustains certain processes (e.g. transport) [5]. (iii) The topology of a network evolves at the same time as the dynamical processes it sustains are going on, and there is a coupling between the two [6]. The main focus of this work is on (ii). In addition, cases (i) and (iii) could be easily addressed but for simplicity reasons we refrain from this at the moment.

Figure 1 gives an example of the problem one has to deal with. Such structures have been studied experimentally in a number of papers (see [7] and references therein). The goal is to find a method that can be used to

describe diffusive transport of particles on a network consisting of M containers (reservoirs) labeled $C_1; \dots; C_M$ of radii R_i connected by tubes of length l_{ij} and radii a_{ij} where $i, j = 1; 2; \dots; M$. It is possible that some tubes are absent and it may happen that tubes join each other forming a junction without any container being present. In such a way one can generate an enormous number of network topologies. In the standard terminology the containers and tubes play the role of nodes and links respectively. Note that each link in Fig. 1 has well defined geometrical properties such as diameter of the tube and length. The theory is developed for the general case where the diffusion constant in each tube can be different, D_{ij} $i, j = 1; \dots; M$ are arbitrary.

For large networks, links connecting opposite sides of the network may be rather long. Accordingly, one can not expect an exponential decay of the number of particles and this is the situation we are mostly interested in. Obviously, to describe such a situation one can attempt to solve the diffusion equation numerically and obtain the distribution function $\langle n; t \rangle$ that describes how particles spread throughout the network. Thus, our formal starting point is the diffusion equation, which has to be solved in the geometry depicted in Fig. 1. The solution of a diffusion equation for such a complicated geometry is a rather demanding task and for large networks it gets highly impractical. In this work we develop a method of calculation that is computationally efficient and can be used to study transport in large networks. Instead of finding the full distribution function $\langle n; t \rangle$ we introduce a set of slow variables that capture the most important aspect of particle transport, the number of particles in each container $N_1(t); N_2(t); \dots; N_M(t)$, and derive equations that describe how they change in time. This is the

Address: Chalmers University of Technology, SE-412 96 Goteborg, Sweden. E-mail: zorank@fy.chalmers.se. Tel. +46 31 772 3186; Fax: +46 31 41 69 84.

central result of the paper.

The details of the dynamics within containers is projected out. In such a way one reduces the amount of information, e.g. the distribution profile of $(\mathbf{r};t)$ within the container can not be traced, but there is an advantage from a computational point of view since the number of dynamical variables is reduced from an infinite number to M . In principle, the distribution of particles in the tubes $(\mathbf{r};t)$ has to be calculated as well but it is possible to describe this part analytically and project it out.

A couple of related problems have been addressed previously in refs. [8, 9, 10, 11, 12]. Escape of a particle through a small hole in a cavity was studied in [8]. The work of [9] deals with the problem of the hole connected to a short tube. The tube length and hole radius are roughly of the same size, mimicking a cell membrane having a thickness greater than zero. A couple of equilibrium cases have also been studied [10, 11, 12]. The papers just indicated treat the intra container dynamics in much more detail than we do. In here, for simplicity reasons, the particle concentration is assumed flat in the container and the validity of this approximation is checked numerically in section VII. In our notation, the studies [8, 9, 10, 11, 12] can be classified as $M = 1;2$ cases. Our main interest is in networks with large M .

Although we deal with a rather simple model based on diffusive transport, apart from obvious relevance for experimental work published in [7], our findings are related to a number of research topics. In the following we discuss few examples.

Most network studies focus on topological issues such as connectivity patterns, the average minimum path between two arbitrary chosen nodes, or the number of neighbors. On the other hand, the study of geometrical aspects of network dynamics has been somewhat neglected. The techniques developed in this work could be used to explore the geometrical side of the problem in a more detail. For example, the transport along the tubes is not instantaneous. The distance covered by diffusion in time t scales as \sqrt{t} , and the geometry of the network (length of the tubes) will undoubtedly have an effect on the transport properties of the network. In particular, when studying properties of the small world networks.

The small world networks have been explored in great detail [1]. They arise in social environments, in the dynamics of the living cell and in the Internet, just to mention a few examples. Despite their large size, the mean shortest distance between two arbitrary nodes (mean path length) is unexpectedly short [13]. Mean path length is expressed in terms of the number of nodes. As an artifact of this, information can be transferred relatively fast throughout the network. However, if the physical length of the tube is used as a measure of length, one has an entirely different situation. The transport of chemicals along the tube is not instantaneous and the length of such large leaps will become a very important factor in the dynamics.

The structures like the one depicted in Fig. 1 can be

used to model transport of molecules in the living cell. A large number of processes happening in the cell are governed by transport of reactants and chemical reactions. In order to avoid a need for excessive storage facilities the chemical compounds are routed in an orderly fashion between various places within and between the cells and the chemical components arrive exactly at the right place at the right time. The setup in Fig. 1 captures this aspect of the cell interior.

Although we exclusively study transport, our model can serve as a platform for reaction-diffusion-based bio-computing devices [14, 15, 16, 17, 18, 19, 20, 21, 22, 23, 24, 25, 26, 27, 28, 29, 30, 31]. For example, studies in [22, 23, 24] deal with networks of chemical reactions where reactors of macroscopic sizes are connected by tubes. The exchange of reactants is mediated through the tubes and controlled by pumps. In this way one establishes a neural-network based device where information is carried by the concentration of reactants. The reactors serve as nodes and tubes as links. The strength of synapses in the network is controlled by pump intensities. It was shown that it is possible to use this setup to carry out pattern recognition. The experimental setup has a computational time of the order of hours and clearly there is an interest of miniaturizing such a device in order to speed it up. For example, micro-scale networks have been already built [7]. A small device allows the removal of external pumping and the transport can be limited to pure diffusion, which is a situation studied in this work.

Our work is also applicable to studies of the reaction-diffusion neuron [25, 26, 27, 28, 29, 30, 31]. The reaction-diffusion neuron is motivated by the biology of nerve cells. The reaction-diffusion neuron is a 2D array of compartments that exchange chemicals by diffusion. External patterns are transformed into chemical internal structures (distribution of reactants) which propagate and react and in such a way process external information. The information is read off by enzymes that are located in the various compartments. When the concentration of reactants exceeds a certain threshold in a compartment with enzyme, the neuron fires. It has been shown that by rearranging the positions of enzymes one can achieve programmability and train reaction-diffusion neuron to recognize certain patterns. At the moment, reactions are not considered in this work but apart from this fact our setup is very similar to a reaction-diffusion neuron.

This paper is organized as follows. In section II the problem is defined and the general results are stated. The derivation of the rate Eq. (3) is explained in sections III and IV where the emptying of a single container into a tube, and emptying of a container into another container through the tube is studied. The single exponential asymptotics of the two container system and related first order rate equations are found and discussed in section V. Up to this point only a two-container system is treated while section VI deals with an arbitrary network topology. Section VII elaborates on the assumption of well stirred containers. A numerical comparison to

the diffusion equation is made. In section V III numerical case studies of various network structures are performed. In particular a three way junction and an example of a larger network are studied. The summary and outline of future work is given in section IX. Technical details are found in the appendices. Appendix A describes the numerical procedure used for solving the rate equations. The rate equations for the cases studied in Section V III are explicitly derived in Appendix C. It can be shown that the presence of tube junctions can be eliminated altogether from the dynamical equations when the time is large. This is demonstrated in Appendix D.

II. PROBLEM DEFINITION AND MAIN RESULT

Describing the particle transport in a network depicted in Fig. 1 is far from trivial and in order to solve the problem several assumptions are made. We assume that (i) particles move solely by diffusion (the fluid in which the particles move stands still) and (ii) particles do not disturb each other. With these assumptions the complicated dynamical problem at hand is reduced to solving the time dependent diffusion equation:

$$\partial_t (\mathbf{r}; t) = r \nabla \cdot (\mathbf{r}) \nabla (\mathbf{r}; t) : \quad (1)$$

Here $\mathbf{r}; t$ is the concentration (particle density) and $\nabla \cdot (\mathbf{r})$ is the diffusion coefficient which may be position dependent. The walls are particle impenetrable

$$\partial_n (\mathbf{r}; t) = 0 \quad (2)$$

where $\partial_n = \hat{n} \cdot \nabla$, and \hat{n} is the unit vector perpendicular to the wall. The total number of particles is a conserved quantity.

Equation (1) could in principle be solved numerically using a brute force approach (e.g. the Finite Element Method or the Finite Difference method). However, the computational cost scales with network size and there is an upper limit to what systems one can handle in such a way. It is more desirable to have a method that could treat large networks: in sections III and IV we will show that it is possible to describe particle transport in terms of a finite number of variables, the number of particles in each container $N_1; \dots; N_M$. Also, it might be easier to understand particle transport in such a setup. The dynamics of $N_i(t)$ $i = 1; \dots; M$ is governed by

$$\begin{aligned} \dot{N}_1(t) = & \sum_{j=1}^M C_{ji} \frac{V_{d-1}(a_{ij})}{V_d(R_j)} R_t \int_0^t dt N_j(t^0) j_i(t-t^0) \\ & - \sum_{j=1}^M C_{ij} \frac{V_{d-1}(a_{ij})}{V_d(R_i)} R_t \int_0^t dt N_i(t^0) [j_{ij}(t-t^0) \\ & - j_{ij}(t-t^0)] \end{aligned} \quad (3)$$

where

$$N_i(t) = N_1(t) + N_{i0}(t) \quad (4)$$

and $\delta(t)$ is the Dirac delta-function, $\int_0^t dt \delta(t) = 1$. Here and in the following the dot over symbol denotes time derivative. The connectivity matrix C_{ij} $i, j = 1, \dots, M$ describes how the nodes are linked (note that $C_{ii} = 0$), a_{ij} is the radius of the tube (link) from i to j and $V_d(R_j)$ is the volume of a d dimensional sphere $V_d(r) = \frac{\pi^{d/2}}{\Gamma(d/2+1)} r^d$ corresponding to container (node) j having radius R_j . N_{i0} denotes $N_i(t=0)$. Equation (3) is derived under the assumption of ideally mixed containers. The rate coefficients are given by

$$\begin{aligned} j_{ij}(t) = & \frac{r}{D_{ij}} \frac{x^i}{t} \\ j_{ij}(t) = & 2 \frac{r}{D_{ij}} \frac{x^i}{t} \exp \left(-\frac{(k_{ij})^2}{D_{ij}t} \right) \\ j_{ij}(t) = & 2 \frac{r}{D_{ij}} \frac{x^i}{t} \exp \left(-\frac{((2k-1)x_{ij})^2}{4D_{ij}t} \right) : \end{aligned} \quad (5)$$

x_{ij} is the link length and D_{ij} is the corresponding diffusion coefficient.

Figure 1 also shows the existence of tube junctions. They are treated by Eq. (3) by letting the container radius coincide with that of the tube. Since the tubes are initially empty, so are junctions, $N_{i0} = 0$. Eqs. (3)–(5) are the central results of this paper and their derivation is a major topic of the subsequent sections.

III. EMPTYING OF A RESERVOIR THROUGH AN INFINITELY LONG TUBE

To derive Eq. (3) we start with the simplest possible case and consider particle escape from a container through an infinitely long tube [see Fig. 2, panel (a)]. The main reason for this is to show how to couple the dynamics of the tube and the container. Also, such setup captures the short time description of the full network problem when the particles escaping the containers do not yet ‘feel’ that the system is closed [the short time dynamics is contained in $\delta(t)$, see Section IV].

The particle concentration $\mathbf{r}; t$ is governed by the diffusion equation supplemented with the boundary conditions that the walls are impenetrable and that $\mathbf{r}; t$ has to vanish for $x \rightarrow 1$. The concentration in the tube and in the container are interoven in a highly non-trivial way through what is occurring at the tube opening. Given that the current density out of the container $j(0; y; z; t)$ is known [see Fig. 2 (a)] one could solve the diffusion problem and find the concentration profile in the container and the number of particles. Furthermore, one could find a relationship

$$j(0; y; z; t) = F[j(0; y; z; t)] \quad (6)$$

where $j(0; y; z; t) = D \lim_{x \rightarrow 0} \frac{\partial}{\partial x} \mathbf{r}(x; y; z; t)$. F is a functional that we know exists but is unlikely to be

found in a closed analytic form. The current at $t = 0$ is a function of the dynamics in both regions and is therefore not known a priori. To find $j(0; y; z; t)$ one has to address the dynamics in the tube as well.

The situation simplifies drastically if it is assumed that the x dependence of the concentration profile in the tube can be decoupled according to

$$c(x; y; z; t) = f(y; z; t) c(x; t); \quad x \geq 0 \quad (7)$$

where $c(x; t)$ is a one-dimensional concentration along the tube and $f(y; z; t)$ is a function that projects the value of $c(x; t)$ onto a radial direction. Thus, by assumption, the radial profile is same for all x . This is of course not true since a density profile at the opening will in time smear out due to radial diffusion. The approximation becomes however better with decreasing tube radius. The decoupling in Eq. (7) effectively maps the tube dynamics onto an one-dimensional diffusion problem. The advantage of this approach is that the solution to a one-dimensional diffusion equation can be found analytically leading to $c(x; t)$.

The $c(x; t)$ is coupled to the concentration in the container as follows. Both concentration and current have to be continuous as one moves from the container into the tube leading to

$$c(0; y; z; t) = f(y; z; t) c(0; t); \quad (8)$$

and

$$j(0; y; z; t) = f(y; z; t) \lim_{x \rightarrow 0^+} \frac{\partial}{\partial x} c(x; t) \quad (9)$$

Taking into account particle conservation at the tube opening leads to

$$\int_{x=0}^{\infty} \frac{\partial}{\partial x} c(x; t) dx = c(0; t) \quad (10)$$

which after using Eq. (8) results in the condition $\int_{x=0}^{\infty} \frac{\partial}{\partial x} c(x; t) dx = c(0; t)$.

The problem has four unknowns $c(0; t)$, $j(0; y; z; t)$, $c(x; t)$ and $f(y; z; t)$ and four equations (6), (8)-(10) and is fully defined. In summary, the problem is solved by finding the solution to the diffusion equation in the container and in the tube, $c(x; t)$ and $c(0; t)$, and then couple them with Eqs. (6), (8), (9) and (10). Please note that $\lim_{x \rightarrow 0^+} \frac{\partial}{\partial x} c(x; t)$ in Eq. (9) can be expressed in terms of $c(0; t)$. Even though the problem is completely defined it is not tractable in this complicated form except in certain special cases. For large networks instead of $c(x; t)$ a more convenient variable is the total number of particles in the container $N(t) = \int_{x=0}^{\infty} c(x; t) dx$ governed by

$$\dot{N}(t) = -J(t) \quad (11)$$

where $J(t)$ is the flow of particles that leave the container through the tube opening $J(t) = \int_{x=0}^{\infty} j(0; y; z; t) dy dz$.

There are two special cases where the current $J(t)$ can be determined analytically in terms of container variables. (i) If the exit is a fully absorbing disk with radius a , the concentration is always zero at the interface $c(0; y; z; t) = 0$. In [32] it is shown that the current J_1 through such disk when placed at an infinite otherwise reflecting wall is $J_1 = 4D_c a c_1$ where c_1 is the particle concentration at infinity and D_c denotes the diffusion constant in the container. A reasonable assumption for the container, at least when the tube radius is smaller than the radius of the container, is that the concentration profile far away from the exit is flat and can approximately be taken to be $N(t) = V_d(R) c_1$. Using this for c_1 yields $J_1(t) = 4D_c a N(t) = V_d(R) J$. (ii) If the opening is completely closed, the current is zero and $c(0; y; z; t) = N(t) = V_d(R) c_1$ [in such a case $N(t) = N(0)$]. A linear interpolation between (i) and (ii) yields

$$c(0; y; z; t) = \frac{N(t)}{V_d(R)} \left(1 - \frac{J(t)}{J_1(t)} \right) \quad (12)$$

where $c(0; y; z; t)$ is assumed constant across the interface. This equation is a simplified version of Eq. (6). Equation (12) implies that the container can be considered as ideally mixed $c(0; y; z; t) = N(t) = V_d(R) c_1$ when the current $J(t)$ is small. The type of networks under investigation are such that the radius of the tube a is small in comparison to the tube length l and the radius of the container R . Small radius implies small current and hence ideally mixed containers. This is verified by numerical calculations in Section VII.

Effectively, the full problem has been mapped on to a very simple geometry depicted in Fig. 2 (b): a one-dimensional line (tube) connected to a point (container). Tube dynamics is characterized by a one-dimensional particle density $c(x; t)$ along the line and all container dynamics, how complicated it may be, has been projected on to a single variable $N(t)$.

It was verified numerically that for a fixed $f(y; z; t)$ is constant to a very good approximation (not shown here). In such case $f(y; z; t) = V_d^{-1}(a)$ and the coupling Eq. (8) becomes

$$c(0; t) = V_d^{-1}(a) \frac{N(t)}{V_d(R)} \quad (13)$$

The concentration profile along the tube [initially empty $c(x; 0) = 0$] is given by the diffusion equation

$$\frac{\partial c(x; t)}{\partial t} = D \frac{\partial^2 c(x; t)}{\partial x^2} \quad x \in [0; l] \quad (14)$$

supplemented with boundary conditions according to Eq. (13) and $c(l; t) = 0$. The solution can be found by the Laplace transform method [33] and is given by

$$c(x; s) = c(0; s) e^{-x \sqrt{s/D}} \quad (15)$$

where $c(x; s) = \int_0^\infty dt c(x; t) e^{-st}$. Integrating Eq. (9) over the tube interface area at $x = 0$ gives

$$J(t) = -D \lim_{x \rightarrow 0^+} \frac{\partial}{\partial x} c(x; t) \quad (16)$$

Combining Eqs. (11), (13) and (16) leads to a rate equation in the Laplace transform space

$$\begin{aligned} sN(s) - N_0 &= \lim_{x \rightarrow 0} \frac{p}{sD} N(s) \frac{V_{d-1}(a)}{V_d(R)} e^{x \frac{p}{s=D}} \\ &= \frac{p}{sD} N(s) \frac{V_{d-1}(a)}{V_d(R)} \end{aligned} \quad (17)$$

where $L[N(t)] = sN(s) - N_0$. It is tempting to rewrite this equation in the time domain in the form of convolution

$$N(t) = \int_0^t dt^0 k(t^0) N(t - t^0) \quad (18)$$

representing a general form of a rate law, where $k(t) = \frac{V_{d-1}(a)}{V_d(R)} L^{-1} \left[\frac{p}{sD} \right]$. However, this is impossible and can be seen in several ways.

First, $\frac{p}{s}$ has no well defined inverse Laplace transform and $k(t)$ that would enter into the rate equation (18) is ill defined. Second, this problem could possibly be resolved by inverting Eq. (15) to obtain $c(x;t)$ and inserting the result into Eq. (16) which leads to

$$J(t) / \lim_{x \rightarrow 0} \frac{\partial}{\partial x} \int_0^t dt^0 \frac{x}{t^{3/2}} e^{x^2 = 4Dt^0} N(t - t^0) : \quad (19)$$

In general $N(t)$ is unknown. To evaluate the expression above in a way that would result in a rate equation involves interchanging derivation and integration. This is only allowed if the integral is uniformly convergent in the interval $x \in [0; 1]$ [34]. It is easy to see from Eq. (19) that this is not the case and the interchange is illegal. Another possibility is to use partial integration but this strategy does not work since one ends up with non-convergent integrals as $x \rightarrow 0$. Thus, Eq. (18) does not exist for a semi-infinite case. Also, it is intuitively clear that one can not observe pure exponential decay since the system is infinite.

For an infinite system an asymptotic rate law of the type $N(t) / N(t)$ simply does not exist. This can also be seen from the exact expression for $N(t)$ which can be obtained from Eq. (17) by solving for $N(s)$ and finding the inverse Laplace transform [33]

$$N(t) = N_0 \exp \left[-D t \frac{V_{d-1}(a)}{V_d(R)} \operatorname{erfc} \left(\frac{p}{s=D} \frac{V_{d-1}(a)}{V_d(R)} \right) \right] : \quad (20)$$

N_0 is the initial number of particles in the container. Using approximation $\operatorname{erfc}(z) \approx \frac{e^{-z^2}}{z}$ for large z gives $N(t) / \frac{1}{t}$.

Due to the complications discussed above the rate

equation has to be stated in terms of $N(t)$

$$\begin{aligned} N(t) &= \frac{V_{d-1}(a)}{V_d(R)} L^{-1} \left[\frac{p}{sD} N(s) \right] \\ &= \frac{V_{d-1}(a)}{V_d(R)} \int_0^t dt^0 N(t^0) \quad (t - t^0) \end{aligned} \quad (21)$$

where

$$N(t) = L^{-1} [sN(s)] = N(t) + N_0(t) \quad (22)$$

and

$$(t) = L^{-1} \left[\frac{p}{sD} \right] = \frac{D}{t} : \quad (23)$$

Please note that it is impossible to rewrite the right hand side of Eq. (21) in such a way that it would solely involve dependence on $N(t)$. When the system is closed (e.g. by adding another container) the situation changes.

IV. A RATE EQUATION FOR A TWO CONTAINER SYSTEM

The system under consideration consists of a one dimensional rod parameterized by a and ℓ connected to two ideally mixed containers having radii R_1 and R_2 depicted in Fig. 3.

The diffusion equation for the tube [initially empty, $c(x;t) = 0$] connected to the two containers at $x = 0$ and $x = \ell$ is given by

$$\frac{\partial c(x;t)}{\partial t} = D \frac{\partial^2 c(x;t)}{\partial x^2} \quad x \in (0; \ell) \quad (24)$$

with boundary conditions analogous to Eq. (13)

$$c(0;t) = N_1(t) \frac{V_{d-1}(a)}{V_d(R_1)}; \quad c(\ell;t) = N_2(t) \frac{V_{d-1}(a)}{V_d(R_2)} : \quad (25)$$

The solution in Laplace transform space is given by

$$c(x;s) = \frac{V_{d-1}(a)}{V_d(R_1)} sN_1(s) \phi_1(x;s) + \frac{V_{d-1}(a)}{V_d(R_2)} sN_2(s) \phi_2(x;s) \quad (26)$$

where

$$\phi_1(x;s) = \frac{\sinh(x \sqrt{s})}{s \sinh(\ell \sqrt{s})} \frac{p}{s=D}; \quad \phi_2(x;s) = \frac{\sinh(x \sqrt{s})}{s \sinh(\ell \sqrt{s})} \frac{p}{s=D} : \quad (27)$$

Matching the current at both ends as in Eq. (16)

$$N_1(t) = -D \lim_{x \rightarrow 0} \frac{\partial}{\partial x} c(x;t) \quad (28)$$

$$N_2(t) = -D \lim_{x \rightarrow \ell} \frac{\partial}{\partial x} c(x;t)$$

yields a set of rate equations in Laplace transform space for the two container system

$$\begin{aligned} sN_1(s) - N_{10} &= sN_1(s) \frac{V_{d1}(a)}{V_d(R_1)} \frac{r}{s} \frac{\cosh \sqrt{\frac{p}{s}} \frac{D}{s}}{\sinh \sqrt{\frac{p}{s}} \frac{D}{s}} \\ &+ sN_2(s) \frac{V_{d1}(a)}{V_d(R_2)} \frac{r}{s} \frac{1}{\sinh \sqrt{\frac{p}{s}} \frac{D}{s}} \\ sN_2(s) - N_{20} &= sN_2(s) \frac{V_{d1}(a)}{V_d(R_2)} \frac{r}{s} \frac{\cosh \sqrt{\frac{p}{s}} \frac{D}{s}}{\sinh \sqrt{\frac{p}{s}} \frac{D}{s}} \\ &+ sN_1(s) \frac{V_{d1}(a)}{V_d(R_1)} \frac{r}{s} \frac{1}{\sinh \sqrt{\frac{p}{s}} \frac{D}{s}} : \end{aligned} \quad (29a)$$

$$(29b)$$

The terms having minus signs are the outflow while the ones having plus signs represent the inflow. A closer look at the rate equations above reveals an important link to the semi-infinite case: the outflow is proportional to $\sqrt{p/s}$ for large t (small s). In other words, the semi-infinite case is recovered as a short time expansion of Eqs. (29) (see Section III). The physical interpretation is that initially, the particles feel as if they were entering an infinitely long tube. This implies that the outflow term can be divided into two parts reflecting this observation

$$q \frac{D}{s} \frac{\cosh \sqrt{\frac{p}{s}} \frac{D}{s}}{\sinh \sqrt{\frac{p}{s}} \frac{D}{s}} (s) + (s) : \quad (30)$$

(s) is taken from Eq. (23) and controls the short time dynamics that resembles the one of the semi-infinite system. (s) describes the asymptotic long time behavior when the particles are 'aware' of the existence of another side and can be found from Eq. (23) and Eq. (30)

$$(s) = \frac{r}{s} \frac{\exp \sqrt{\frac{p}{s}} \frac{D}{s}}{\sinh \sqrt{\frac{p}{s}} \frac{D}{s}} : \quad (31)$$

The inflow rate is labeled (s)

$$(s) = \frac{r}{s} \frac{1}{\sinh \sqrt{\frac{p}{s}} \frac{D}{s}} : \quad (32)$$

The inverse Laplace transforms of (s) , (s) and (s) are shown in Eq. (5) and depicted in Fig. 4. The long time behavior of (t) and (t) can be found from a small s expansion of the Eqs. (31) and (32)

$$\begin{aligned} (t) &= \frac{D}{\sqrt{t}} \\ (t) &= \frac{D}{\sqrt{t}} \left(1 - \exp \left(-\frac{6D}{\sqrt{t}} \right) \right) : \end{aligned} \quad (33)$$

Taking the limit $t \rightarrow 1$ yields

$$(1) = \frac{D}{\sqrt{t}} \quad (1) = \frac{D}{\sqrt{t}} : \quad (34)$$

It is more convenient to express the rate Eqs. (29) in time domain

$$\begin{aligned} N_1(t) &= \frac{V_{d1}(a)}{V_d(R_2)} \int_0^t dt N_2(t^0) (t - t^0) \\ &+ \frac{V_{d1}(a)}{V_d(R_1)} \int_0^t dt N_1(t^0) (t - t^0) + (t - t^0) \end{aligned} \quad (35a)$$

$$\begin{aligned} N_2(t) &= \frac{V_{d1}(a)}{V_d(R_1)} \int_0^t dt N_1(t^0) (t - t^0) \\ &+ \frac{V_{d1}(a)}{V_d(R_2)} \int_0^t dt N_2(t^0) (t - t^0) + (t - t^0) \end{aligned} \quad (35b)$$

(t) and (t) are not present in the rate equation for the semi-infinite case (see Eq. 21) and arise only when the system is finite.

A numerical solution to Eqs. (35) is shown in Fig. 5 (see Appendix A for a more elaborate discussion regarding the numerical procedure). The number of particles decays exponentially which is verified in Fig. 6 where the straight line attained after some time is the evidence of a single exponential decay. The figure also shows a non-exponential regime for small t , described by (t) . Terms proportional to (t) are in the following referred to as $-term s$.

For small t particles rush into the tube with a large current. At $t = 0$ the current is infinite, $\lim_{t \rightarrow 0} N_1(t) = 1$. Thus, exactly at $t = 0$ it is impossible to define the exit rate from container and such situation extends to any other time instant. In strict mathematical sense, it is impossible to define exit rate from the container for any $t > 0$ (when the concentration profile at the tube opening is different from zero). This can be illustrated on a simple example. Let V be a volume divided into two sub-volumes V_1 and V_2 such that V_1 and V_2 touch each other and exchange particles by diffusion. The dynamical variables of interest are the total number of particles in each sub-volume $N_1(t)$ and $N_2(t)$. The goal is to derive some kind of rate equation for $N_1(t)$ and $N_2(t)$. We focus on the flow from V_1 to V_2 . In a small time interval one will have $N_1(t + \Delta t) / N_1(t) (1 - \Delta t)$ and $N_2(t + \Delta t) / N_2(t) + N_1(t) \Delta t$, where Δ and Δ are numerical constants. The effective exchange rate that describes the flow from V_1 into V_2 is given by

$$k_{21}(t) = \lim_{\Delta t \rightarrow 0} \frac{N_2(t + \Delta t) - N_2(t)}{N_1(t) \Delta t} / \lim_{\Delta t \rightarrow 0} \Delta t = 2 \quad (36)$$

which is infinite. At any time instant t an infinite amount of particles (per unit time) is rushing from V_1 into V_2 (and vice versa). However, the inflows from V_1 to V_2 and the other way around cancel each other out resulting in a finite net flow giving smooth curves for $N_1(t)$ and $N_2(t)$. $t = 0$ is special since there is no counterflow from V_2 to V_1 which explains why $\lim_{t \rightarrow 0} N_1(t) = 1$.

The non-exponential regime grows with tube length D and might play a significant role in studying transport processes in networks having long connections. For large

times (t) and (t) start to dominate and one observes exponential decay. It will be shown in Section V how to derive rate equations that describe this regime.

V. ANALYSIS OF THE GENERAL RATE EQUATION: EMERGENCE OF A SINGLE EXPONENTIAL SOLUTION

It is intuitively clear that in the case of the two-node network discussed in previous section one should have an exponential decay (growth) for the number of particles in the container C_1 (C_2) (see Figs. 5 and 6): asymptotically the time dependence of $N_1(t)$ and $N_2(t)$ is given by

$$N_{1,2}(t) = N_{1,2}(1) + A_{1,2} \exp(-t/\tau) \quad (37)$$

where $1/\tau$ is the decay exponent that governs the late time asymptotics and $A_{1,2}$ is the amplitude of decay. This fact is not easily predicted from the form of the general rate equation given in (3). To understand the emergence of such behavior a more thorough investigation of Eq. (46) is needed.

To obtain the exact value of the decay exponent one has to study the structure of poles of $N_{1,2}(s)$. The poles fully determine the form of $N_{1,2}(t) = \sum_{p=0}^1 a_p e^{s_p t}$ where a_p is the residue of $N_{1,2}(s)$ at pole s_p . The values of $N_{1,2}(1)$ are determined by the $p=0$ term ($s_0=0$). The exponential decay rate is determined by

$$1/\tau = -s_1 \quad (38)$$

Rewriting Eqs. (29) in matrix form yields

$$s\mathbf{N}(s) - \mathbf{N}_0 = \mathbf{M} \mathbf{N}(s) \quad (39)$$

where

$$\mathbf{N}(s) = [N_1(s); N_2(s)]^T; \mathbf{N}_0 = [N_{10}; N_{20}]^T \quad (40)$$

and

$$\mathbf{M} = \begin{pmatrix} \frac{V_{\text{tube}}}{V_d(R_1)} \coth q & \frac{V_{\text{tube}}}{V_d(R_2)} \frac{1}{\sinh q} \\ \frac{V_{\text{tube}}}{V_d(R_1)} \frac{1}{\sinh q} & \frac{V_{\text{tube}}}{V_d(R_2)} \coth q \end{pmatrix} \quad (41)$$

with $q^2 = s^2 D$ and $V_{\text{tube}} = V_{d1}(a)$. The poles are calculated from $\det(s\mathbf{M} - \mathbf{M}) = 0$ since $\mathbf{N}(s) = (s\mathbf{M} - \mathbf{M})^{-1} \mathbf{N}_0$ and $(s\mathbf{M} - \mathbf{M})^{-1} / 1 = \det(s\mathbf{M} - \mathbf{M})$. Evaluating $\det(s\mathbf{M} - \mathbf{M}) = 0$ gives

$$q^2 + q \frac{V_{\text{tube}}}{V_d(R_1)} + \frac{V_{\text{tube}}}{V_d(R_2)} \coth q + \frac{V_{\text{tube}}^2}{V_d(R_1)V_d(R_2)} = 0 \quad (42)$$

Equation (42) is a transcendental equation and has many solutions q_p that determine the value of the poles $s_p = -q_p^2 D$ where $p = 1, 2, \dots, 1$ and in particular

$$s_1 = -\frac{q_1^2 D}{\tau} \quad (43)$$

that, together with Eqs. (38), gives a relationship between q_1 and the decay rate $1/\tau = q_1^2 D$. Note that q_1^2 has been factored out from Eq. (42) and $s_0 = 0$ ($q_0 = 0$) is the additional pole that determines the values of $N_{1,2}(1)$. Also, note that q_1 depends only on parameters describing geometry of the network.

Apart from determining the structure of the poles, Eqs. (39)–(41) are a good starting point for classifying various schemes for obtaining approximative forms of the rate Eqs. (35). Equations (35) do not have the form of the general rate law stated in Eq. (18) (due to the presence of the t -terms). Such a rate law would be easier to understand intuitively. For example, the emergence of the single exponential decay could be seen more easily in Eq. (18) than in Eqs. (35). Also, an approximative form might be easier to implement numerically, though at the cost of a lower accuracy at the end. The idea is to perform a small s expansion of Eq. (39) based on a desired accuracy. In here we consider two cases.

(a) Lowest order expansion: Performing the expansion

$$q \coth q \approx 1 - \frac{q}{\sinh q} \approx 1 \quad (44)$$

of M in Eq. (41) leads to a matrix that is constant, and taking the inverse Laplace transform of Eq. (39) gives the following set of rate equations

$$N_1(t) = N_2(t) = V_{\text{tube}} \frac{D}{V_d(R_2)} \frac{N_2(t)}{V_d(R_2)} - \frac{N_1(t)}{V_d(R_1)} : \quad (45)$$

These equations were already stated in ref. [10]. It is interesting to see that they emerge as a special case of the scheme discussed here. Also, Eq. (45) can be obtained by following another route. Performing partial integration of Eqs. (35) with terms containing t omitted leads to the exactly the same form of rate equations as given in (45). This procedure is discussed below.

The t -terms are only present when the system is infinite. Since the problem is finite, terms proportional to t will be sub-leading for large t . This can be seen from a small s (large t) expansion of Eqs. (23) and (31) [38]. Also, partial integration of the t -terms is impossible since the derivative of t is proportional to $t^{-3/2}$ and diverges when $t \rightarrow 0$.

Omitting t -terms in Eqs. (35), and performing partial integration leads to

$$N_1(t) = \frac{V_{d1}(a)}{V_d(R_2)} \int_0^t dt N_2(t-t) - (t^0) \quad (46a)$$

$$N_2(t) = \frac{V_{d1}(a)}{V_d(R_1)} \int_0^t dt N_1(t-t) - (t^0) \quad (46b)$$

Since $\phi(t)$ is peaked for small t (see Fig. 4), the contribution to the integrals (convolutions) stem mainly from small values of t^0 which justifies the following approximation

$$\int_0^t dt^0 N_{1,2}(t-t^0)\phi(t^0) \approx N_{1,2}(t)\int_0^t dt^0 \phi(t^0) = N_{1,2}(t)\phi(t) : \quad (47)$$

where $\phi(0) = 0$ was used. The same applies for $\phi(t)$. Using Eq. (47) in (46) leads to

$$N_1(t) = \frac{V_d + 1}{V_d(R_2)} N_2(t) \phi(t) - \frac{V_d + 1}{V_d(R_1)} N_1(t) \phi(t) \quad (48a)$$

$$N_2(t) = \frac{V_d + 1}{V_d(R_1)} N_1(t) \phi(t) - \frac{V_d + 1}{V_d(R_2)} N_2(t) \phi(t) : \quad (48b)$$

Inserting (48a) and (48b) found in Eq. (34) into (48) yields (45). This example shows how the ϕ -terms disappear from the description when the system is finite. However, contrary to the partial integration method, the expansion of Eq. (39) gives a more systematic and controlled approach.

Equation (45) is simple and computationally efficient. It could be easily used to describe large networks. However, it has several drawbacks that can be identified. The solution to Eq. (45) is given by

$$N_{1,2}(t) = N_{1,2}(1) = N_{1,2}(0) = N_{1,2}(1) \exp(-t/\tau_{1,2}) : \quad (49)$$

The decay rate $\tau_{1,2}^{-1} = \alpha_{1,2}^2 D = \alpha^2$ is determined by

$$\alpha_{1,2}^2 = \frac{V_{\text{tube}}[V_d(R_1) + V_d(R_2)]}{V_d(R_1)V_d(R_2)} : \quad (50)$$

The number of particles in each container as $t \rightarrow 1$ is

$$\frac{N_1(1)}{V_d(R_1)} = \frac{N_2(1)}{V_d(R_2)} = \frac{N_{10} + N_{20}}{V_d(R_1) + V_d(R_2)} : \quad (51)$$

Equation (51) is not correct. The correct values for $N_{1,2}(1)$ are given by

$$\frac{N_1(1)}{V_d(R_1)} = \frac{N_2(1)}{V_d(R_2)} = \frac{N_{10} + N_{20}}{V_d(R_1) + V_d(R_2) + V_{\text{tube}}} \quad (52)$$

The discrepancies between Eq. (51) and (52) become increasingly important for long tubes which are likely to occur in large networks. For example, in a case where the tube and reservoir volumes are equal, Eq. (51) predicts $N_1(1) = N_2(1) = N_{\text{tot}}/2$, $N_{\text{tot}} = N_{10} + N_{20}$, while the exact result from Eq. (52) is $N_{\text{tot}}/3$. The particle decay exponent given in Eq. (50) only holds when $V_{\text{tube}} \rightarrow 0$. It strongly deviates from the exact value when the tube is long (see Fig. 7).

(b) Higher order expansion: Using the expansion

$$q \coth q = 1 + \frac{q^2}{3} - \frac{q}{\sinh q} + 1 \quad (53)$$

for M , inserting in Eq. (39) and taking inverse Laplace transform, leads to a set of rate equations (given in Appendix B) that are unsatisfactory due to the following

reasons. First, they predict a spurious jump in $N_{1,2}(t)$ as $t \rightarrow 0$, and the limiting values $N_{1,2}(1)$ are not correct. Second, the rate exponent that results from these equations is not that accurate. This particular example shows that it is important to have a balanced expansion for elements of M . For example, instead of expanding $q \coth q$ directly one has to expand $\sinh q$ and $\cosh q$ separately in such a way that same powers in the numerator and denominator are obtained. When this strategy is followed a much better approximation is obtained as shown below.

The next order expansion, gives correct limits for $N_{1,2}(t)$ when $t \rightarrow 0$ and $t \rightarrow 1$ and leads to a relatively accurate value for the decay exponent. Using the expansion

$$q \coth q = \frac{1+q^2/2}{1+q^2/6} = \frac{q}{\sinh q} = \frac{1}{1+q^2/6} \quad (54)$$

in M gives the following set of equations

$$\begin{aligned} N_1(t) = & N_1(t) \frac{3D}{V_d(R_1)} \frac{V_{\text{tube}}}{V_d(R_1)} \\ & + \frac{12D^2}{V_d(R_1)} \frac{V_{\text{tube}}}{V_d(R_1)} \int_0^t dt^0 N_1(t-t^0) \exp\left(-\frac{6Dt^0}{V_d(R_1)}\right) \\ & - \frac{6D^2}{V_d(R_2)} \frac{V_{\text{tube}}}{V_d(R_2)} \int_0^t dt^0 N_2(t-t^0) \exp\left(-\frac{6Dt^0}{V_d(R_2)}\right) \end{aligned} \quad (55a)$$

$$\begin{aligned} N_2(t) = & N_2(t) \frac{3D}{V_d(R_2)} \frac{V_{\text{tube}}}{V_d(R_2)} \\ & - \frac{12D^2}{V_d(R_2)} \frac{V_{\text{tube}}}{V_d(R_2)} \int_0^t dt^0 N_2(t-t^0) \exp\left(-\frac{6Dt^0}{V_d(R_2)}\right) \\ & + \frac{6D^2}{V_d(R_1)} \frac{V_{\text{tube}}}{V_d(R_1)} \int_0^t dt^0 N_1(t-t^0) \exp\left(-\frac{6Dt^0}{V_d(R_1)}\right) \end{aligned} \quad (55b)$$

Solving $\det(s - M) = 0$ to get hold of the decay exponent in analytical form becomes in this case rather tedious since finding the value q amounts to finding a root of a fourth degree polynomial. The calculation simplifies somewhat if equal container volumes are considered, $V_d(R_1) = V_d(R_2) = V_d$. In such a case one has

$$\alpha_{1,2}^2 = \frac{1}{2V_d} \left[\beta(2V_d + V_{\text{tube}}) \pm \sqrt{3(12V_d^2 - 4V_d V_{\text{tube}} + 3V_{\text{tube}}^2)} \right] \quad (56)$$

The main findings of this section are summarized in Figs. 5, 6 and 7. Figures 5 and 6 depict a numerical solution of Eq. (35) (solid line) compared with the approximations discussed in this section for a case where the tube and container volumes are equal. Figure 7 shows a detailed analysis of the decay rate.

For very short times there is a difference between Eqs. (55) and (35) in Fig. 5 and 6. These arise due to the partial elimination of ϕ -terms. For example, Eq. (55) does not predict $\lim_{t \rightarrow 0} N_1(t) = 1$ [Fig. 5, the dashed line lies above the solid line near $t = 0$ for curves depicting $N_1(t)$]. This is the reason why the curve for $N_1(t)$

obtained from Eq. (55) underestimates the emptying of container C_1 . This effect is more pronounced for the $N_1(t)$ coming from Eq. (49). There, the terms are eliminated altogether [Fig. 5, the dotted line depicting $N_1(t)$ lies above solid and dashed lines]. Also, Figure 5 shows that there is a large error in $N_{1;2}(1)$ for curves obtained by Eqs. (45).

In Fig. 6 the natural logarithm of $N_1(t) - N_1(1) = N_{\text{tot}}$ is shown. For short times the dynamics is not exponential but after some time a straight line is attained which is the evidence of single exponential behavior. The curve corresponding to Eq. (49) (dotted line) does not predict the correct decay exponent which is manifested in a different slope. The decay exponent predicted by Eq. (55) is a better estimate for the decay rate: the slopes of the dashed and solid lines more or less coincide. This fact is shown more clearly in Fig. 7.

Figure 7 depicts the dependence of q_1^2 as a function of the tube volume. The numerical solution to Eq. (42) (solid line), which gives the exact value of the decay exponent, is compared to the values of $q_{1;a}^2$ (dotted line) and $q_{1;b}^2$ (dashed line). All three cases work well when $V_{\text{tube}} \rightarrow 0$. As the tube volume increases $q_{1;a}^2$ deviates more and more from q_1^2 . The same holds for $q_{1;b}^2$, though its value lies much closer to q_1^2 . For example, when all volumes are equal $q_1 = 1.71$ and $q_{1;b} = 1.63$ while $q_{1;a} = 2$.

In this section methods of finding rate equations and decay exponents for the two container problem was deduced. Figures 5, 6 and 7 show that for increasing tube volumes the rate equations given in Eq. (49) are not capable of describing the dynamics. The approximation given in Eq. (55) works better. For short time dynamics none of the developed methods are valid and the full rate Eq. (3) is the only alternative. In the subsequent section all rate equations discussed up to this point will be extended to work for any network structure.

VI. THE GENERAL EXPRESSION

In this section results and methods obtained and developed for two-node network will be extended to work for any network structure. The complete dynamics for the two-node network is formulated in Eq. (35). For an arbitrary network the outflow (OUT) from container i to container j is proportional to $\dot{N}_{ij}(t) + \dot{N}_{ji}(t)$ and the inflow (IN) from container j to container i is proportional to $\dot{N}_{ji}(t)$:

$$\text{OUT}_{i \rightarrow j} = \frac{V_{d-1}(a_{ij})}{V_d(R_i)} \int_0^t dt N_i(t^0) - N_j(t - t^0) + N_j(t - t^0) \quad (57a)$$

$$\text{IN}_{j \rightarrow i} = \frac{V_{d-1}(a_{ji})}{V_d(R_j)} \int_0^t dt N_j(t^0) - N_i(t - t^0) \quad (57b)$$

This implies

$$N_i(t) = \sum_{j \neq i}^X C_{ij} [\text{IN}_{j \rightarrow i} - \text{OUT}_{i \rightarrow j}]; \quad i = 1; \dots; M \quad (58)$$

where C_{ij} is the conductivity matrix discussed in Section II. The final result is stated in Eq. (8).

It was argued earlier that if the tube volume is small a very simple first order rate equation can be stated. It is found in Eq. (45). Extending this equation to the case of arbitrary topology yields

$$N_i(t) = \sum_{j \neq i}^X C_{ij} V_{d-1}(a_{ij}) \frac{D_{ij}}{V_d(R_j)} \frac{N_j(t)}{V_d(R_j)} - \frac{N_i(t)}{V_d(R_i)} \quad (59)$$

Note the symmetry relations $a_{ij} = a_{ji}$, $V_{ij} = V_{ji}$ and $D_{ij} = D_{ji}$.

If a more sensitive solution is desired, a set of equations of the type (55) is suggested. An extension of this equation is shown below

$$\text{OUT}_{i \rightarrow j} = N_i(t) \frac{3D_{ij} V_{d-1}(a_{ij})}{V_{ij} V_d(R_i)} \int_0^t dt \exp \left[-\frac{6D_{ij} t^0}{V_{ij}} \right] N_i(t - t^0) \quad (60a)$$

$$\text{IN}_{j \rightarrow i} = \frac{6D_{ji}^2 V_{d-1}(a_{ji})}{V_{ji} V_d(R_j)} \int_0^t dt \exp \left[-\frac{6D_{ji} t^0}{V_{ji}} \right] N_j(t - t^0) \quad (60b)$$

Inserting Eq. (60) in Eq. (58) yields an approximate form of rate equations for an arbitrary network.

In previous section we investigated differences between Eqs. (57), (59) and Eq. (60) using the two-node network as a study case ($M = 2$). It is expected that the findings of previous section also apply for larger networks. This analysis is not conducted here. Having general expressions at hand more complicated network structures can be investigated. However, the assumption of well stirred containers will be discussed first since it is crucial for the derivation of the rate equations (3).

VII. THE ASSUMPTION OF IDEALLY MIXED CONTAINERS

An ideally mixed container has no concentration gradients. If a particle has entered, it can be found anywhere within the compartment with equal probability. In reality, a diffusing particle examines the compartment in a random walk fashion until an opening is found. There it has a possibility to escape and change the concentration. If the tube radius is small ($a = R - 1$), a significantly longer time is required to find an opening and escape than to examine the majority of the compartment. The time needed to examine the majority of the compartment is called mixing time and is given by $\tau_{\text{mix}} = \frac{R^2}{D}$. The time of finding a specific place or target having radius a is

given by $\tau_{\text{target}} = \frac{R^2}{D} \frac{R}{a}$ [2]. For cubic compartments the radius of the sphere R is replaced by the edge length, in this case $2R$ (see Fig. 8). Thus, we argue that if $a = R$ then $\tau_{\text{mix}} \approx \tau_{\text{escape}}$ and the containers can be considered ideally mixed at all times [39]. This is supported by numerics.

Figure 8 (b) shows a numerical solution of the diffusion equation in two dimensions in a geometry depicted in Fig. 8 (a). The solution clearly shows that the assumption of well stirred containers becomes very good for $a=R$, even for skewed initial distributions. The solution to the diffusion equation was found using a standard implicit finite difference discretization method [35].

In Fig. 8 (b) one observes a systematic discrepancy: the assumption of ideally mixed containers tends to overestimate the decay rate. This derives from the fact that the assumption of well stirred containers overestimates the number of particles at the tube inlet leading to a larger exit rate.

V III. CASE STUDIES

Up to this point the two node network was the only example discussed. It was used as elementary building block when constructing the rate equation (3). Such network is rather simple and does not offer any spectacular behavior. In this section more complicated structures will be studied that are shown in Figs. 9 and 16: Two realizations of a three-node network are studied first, case 1 and 2, depicted in Fig. 9 (a) and (b). They possess one more level of complexity than the two-node network shown in Fig. 3. Case 3, Fig. 9 (c), is a four-node network that has a T-shape structure. Case 4, Fig. 9 (d), has the shape of a star and involves a tube junction. It will be shown that the transport properties of this structure can be controlled in such way that it might serve as a diffusion-based transistor. These three and four node-networks, despite being rather simple, exhibit a large variety of outputs. Case 5, Fig. 16, demonstrates the transport properties for larger networks that are impossible to predict without using Eq. (3). When solving Eq. (3) numerically the containers and the tubes are considered three dimensional. Moreover, the diffusion coefficients D_{ij} and the tube radii a_{ij} were kept the same for all tubes. All graphs are scaled with the total number of particles in the system $N_{\text{tot}} = \sum_{i=1}^M N_i(0)$.

Case 1: The Line. Three reservoirs are lined up on a straight line as depicted in Fig. 9 (a). The transport equations for this system can easily be written down using Eq. (3) and are listed in Appendix C 1. A numerical solution is shown in Fig. 10. This three-node system exhibits a new characteristic that can not be found in the two node network. The curve depicting the number of particles in the middle container (solid line) has a maximum (an extremum) point.

The extremum point is a manifestation of an unbalance between inflow and outflow in the middle container. This unbalance derives from an asymmetry in the structure and arise only when $\lambda_{12} < \lambda_{23}$ or $V_1 < V_3$. This provides a possibility of designing the output pattern through simple geometrical changes in the structure. Fig. 11 is a simple demonstration of this design possibility where λ_{12} is varied so that the arrival time of the maximum of $N_2(t)$, depicting the number of particles in the middle compartment C_2 , is changed. The picture also shows that an increase in λ_{12} results in both an increased arrival time and a wider peak. The height of the maximum is controlled by the value V_2 . A decrease in V_2 suppresses the peak and vice versa.

Case 2: The Triangle. The connectivity of the line is changed by adding an extra link between containers C_1 and C_3 so that it forms the shape of a triangle, as shown in Fig. 9 (b). The rate equations are derived in Appendix C 2 and a numerical solution is shown in Fig. 12. The initial distribution of particles, see the inset in Fig. 12, is chosen in such a way that a minimum is produced in the curve depicting the number of particles in container C_2 .

The extremum point can be enhanced or removed completely in the same way as was demonstrated for case 1. Such minimum will be absent unless the geometry and initial distribution of particles are tailored in a specific way. In general, such sensitivity of geometrical changes and changes in the location where particles are injected is observed for all cases studied in this section.

The triangle structure studied here exhibits shorter equilibrium process than the linear structure considered previously [see Fig. 9 (a)]. In the case of a triangle structure particles can spread more efficiently due to the additional routing possibility $C_1 \rightarrow C_3$.

Case 3: The T-Network. It is interesting to see how the behavior of the cases 1 and 2 changes when a new node is added to the network. In here we study a situation where an extra node C_4 is connected to container C_2 in the structure depicted in Fig. 9 (a). In such a way one gets a T-shaped (star) network shown in Fig. 9 (c). This alternation of structure leads to a significant change in behavior, as shown in Fig. 13. When compared to the cases 1 (one maximum) and 2 (one minimum) the curve depicting $N_2(t)$ exhibits an additional extremum point: both minimum and maximum are present simultaneously. The right inset in Fig. 13 emphasizes this fact.

This scheme could be carried out further adding on more and more reservoirs and adjusting the lengths and the initial distribution so that the peaks arrive in consecutive order, possibly produce a wave-like behavior. However, since the spread of the peaks increases with increasing tube length, it might be numerically quite difficult to see when the extremum points occur or even if they actually exist.

Case 4: The Junction. The next interesting network to consider is the one with a junction present as depicted in Fig. 9 (d). A particular example of a three way junction is studied. The network is built up by three reservoirs and three tubes. The ends of the tubes coincide to form a junction. To obtain the transport properties of such a network we start from the structure studied in case 3 shown in Fig. 9 (c). The junction is obtained by reducing the radius of container C_2 in the middle until its radius is roughly equal to the radii of the surrounding tubes, see Fig. 14. The rate equations describing the junction properties have the same form as the equations describing case 3 (listed in the appendix C 3) with the substitution $V_d(R_3) \rightarrow V_d(a)$. The equations are not given in order to save space.

A numerical solution of the rate equations for the junction is shown in Fig. 15. This structure allows control of the particle flow between V_1 and V_3 by adjusting the volume V_2 and the length l_{24} (see Fig. 14). This setup could function as a diffusion based transistor. For example, by making l_{24} shorter than l_{34} , compartment C_2 will initially attract diffusing particles from C_1 to a greater extent than C_3 causing a time delay in the particle arrival into container C_3 .

This fact is illustrated in Fig. 15 where the maximum in the curve for the number of particles in container C_2 (solid line) indicates an initial accumulation of particles in C_2 : $N_2(t) = N_{tot}$ rises from 0 to 0.5 in the interval $t = 0$ to $Dt = l_{24}^2 = 5$. In this interval container C_2 accumulates the majority of the particles released from container C_1 . After the peak has been reached the particles accumulated in C_2 are released into C_3 : $N_2(t) = N_{tot}$ continuously drops from value of 0.5 after $Dt = l_{24}^2 = 5$. By changing l_{24} the curve for $N_2(t)$ can be manipulated exactly in the same way as done in Fig. 11, but such analysis is not repeated.

For large networks involving junctions it might be desirable to decrease the number of equations required to solve the transport problem. It is demonstrated in Appendix D that the presence of the junctions can be eliminated altogether when investigating dynamics in the $t \gg 1$ regime for structures having large container volumes (a R_i , $i = 1; \dots; M$). Equations (D 8)–(D 10) show this explicitly for the three node junction studied here.

The four cases studied up to now show that the transport dynamics is very sensitive to geometrical changes and to the locations where particles are injected. Small variations in tube lengths and container volumes lead to unpredictable changes in curves depicting the time dependence of the number of particles in each container (Figs. 10, 12, 13 and 15). Also, the shapes of the curves differs significantly from a single exponential decay.

Case 5: Large Network. With some experience one could predict the transport behavior of the networks considered so far. Finally, to demonstrate the power of the method we study a case of a network that is built up

by seven containers, 9 tubes and a 4-way junction. It is impossible to predict the transport behavior of such a network without a numerical calculation. Figure 17, panels (a)–(c), shows numerical solutions of Eq. (3) for the network depicted in Fig. 16. Different initial distributions are used and are introduced into inset of all figures. The darker the container appears the more particles are injected into it.

The dynamics is evidently quite complex and all possible characteristics that were forced upon the other cases are present. There is an exponential growth and decay as well as curves having one or more extremum points. The different transport behavior shown in Fig. 17 stem only from different initial conditions. If the structure no longer remained fixed even more complicated patterns could be produced, only the imagination sets the limits.

IX. CONCLUDING REMARKS

We introduced a generic model for a diffusive particle transport in large networks made of containers and tubes. The diffusion equation that describes the distribution of particles $(\mathbf{r}; t)$ throughout the network was taken as a starting point. To obtain $(\mathbf{r}; t)$ the full diffusion equation has to be solved and, in principle, this amounts to dealing with an infinite amount of variables. Solving the diffusion equation for large networks is a formidable task. Also, an analytical calculation is out of question. Standard numerical procedures that uses various discretization methods are likely to become impractical. Therefore, instead of calculating $(\mathbf{r}; t)$ explicitly, we followed another route and developed a theoretical technique to solve the transport problem using finite number of variables $N_1(t); \dots; N_M(t)$ that describe the number of particles in each container. First, a set of rate equations was derived for the two-node network and second, they were generalized to work for an arbitrary network structure. In such a way we obtained the rate equations that govern dynamics of $N_1(t); \dots; N_M(t)$. These equations are summarized in Eq. (3) and are the central result of the paper.

The transport equations were found by study the exchange of chemicals between the container and the tube. It was demonstrated in Section III how to couple the dynamics in the containers and tubes, as stated in Eqs. (6) and (8)–(10). However, the coupling is too complicated to be carried out in practice in the original form. Several approximations were made in order to make such scheme doable.

The tubes were assumed to be one dimensional lines (see Eq. 8), and the transport in the tubes was described in terms of a one dimensional diffusion problem involving the concentration profile along the line $c(\mathbf{x}; t)$. The expression for $c(\mathbf{x}; t)$ can be found analytically using e.g. Laplace transform technique. In such a way the tubes were eliminated from the problem.

The dynamics in the container is not tractable ana-

lytically but it was argued that when the tube radii are smaller than any other length scales in the system (e.g. tube lengths or container radii) the containers can be treated as ideally mixed at all times. This assumption was verified numerically in Section V II, and simplifies all intra-container dynamics to one dynamical variable: the total number of particles in a given compartment.

Evidently much of the container dynamics has been neglected but the coupling is formulated in such a way that a more detailed description can be developed should there be a need for that. For example, the container dynamics could be better treated by using the techniques presented in e.g. [10], or by further exploration of the coupling equations (6) and (8)–(10). For example, one could keep the second term in the right hand side of Eq. (12) and use $\partial_0 y; z; t = N(t) = V_d(R) \quad J(t) = 4D_c a$ instead of $\partial_0 y; z; t = N(t) = V_d(R)$. This procedure would lead to similar rate equations as presented here with different forms for $\langle t \rangle$, $\langle t \rangle$ and $\langle t \rangle$.

Initially the particles feel as if they are escaping from the container into an infinitely long tube. In this regime the number of particles in the container decays non-exponentially. We have identified terms in the rate equations describing this behavior: all terms in Eq. (3) proportional to $\langle t \rangle$ dominate when time is small. This non-exponential regime grows with increasing tube length and crossover time for this regime scales as $\ell^2 = D$. Also, terms containing $\langle t \rangle$ contain solely dependence on $N_1(t)$ and can not be rewritten in the form that would involve $N_1(t)$. Accordingly, it is impossible to rewrite Eq. (3) so that it adopts a form of a general rate law (see Eq. 18). These issues were discussed in Section III. The bottleneck lies in the definition of transport rate which, in principle, is an ill-defined quantity (see discussions at the end of sections III and IV).

Eventually, for large times the decay is exponential. In such regime term proportional to $\langle t \rangle$ can be neglected in the rate Eq. (3). Other terms proportional to $\langle t \rangle$ and $\langle t \rangle$ can be rewritten in the form of a general rate law, leading to Eqs. (59) and (60). We showed that Eq. (59) is a special case of the general approximation scheme developed in Section V: starting from rate Eq. (3) in Laplace transform space we developed a series of approximations that can be used to systematically describe the asymptotic regime, resulting in Eq. (60). Also, we have developed a procedure that can be used to eliminate junction points for large times which reduces the number of variables further (see Appendix D).

A already simple case studies that were used to illustrate the workings of the method exhibit interesting behavior. For example, one can identify three types of curves that appear in the plots depicting the time dependence of the particle number in each container (Figs. 10–13 and 15). Type I curves occur for the two node network. These lack extremum points and the particle number either strictly rises or drops to saturate to asymptotic values. Type II curves have one maximum or minimum, and type III curves can have more and these are the most interesting.

Type II and type III curves normally describe the particle number for the container in the network interior.

The existence of type I curves for large networks suggests that it could be possible to understand the transport between two nodes in terms of an effective two node network where a complicated structure of links and containers in between two nodes is mapped onto an effective link connecting them. One can raise a more general question: what is the smallest network that would have the same transport properties as some sub-structure of a given large network? For example, if one is interested in only three nodes of the structure depicted in Fig. 16, e.g. C_5, C_7 and C_8 , is there a star-type network, e.g. as the one depicted in Fig. 9 (c) or (d), that would have equivalent transport properties?

The presence of type II and type III curves indicates the possibility that there might be curves that possess a larger number of extremum points. These are likely to occur in larger networks. We can of course manually enhance certain properties as height and width of peaks. This will however become more and more complicated as the network size increases. Problem is that the peaks that occur later have larger width and might be harder to see. For design purposes, it is therefore necessary to build a learning mechanism or a search engine, on top of our existing software, to select certain characteristics in the curves depicting time evolution of $N_1; \dots; N_M$. Furthermore, to exploit such effects one has to amplify them in some way. At the moment our study deals with transport only, but reactions in the containers can be included as well, and they could be tailored to amplify such effects (e.g. by choosing a reaction of enzymatic type).

The networks studied in here could be applied in many ways. Perhaps the most interesting application would be to use networks to perform some kind of bio-chemical computing, for example pattern processing. Similar experimentally devised structures have already been used to simulate a neural network [36]. Also, we can easily incorporate the ideas of reaction-diffusion neuron [27] in our model.

We have considered diffusive non-interacting point particles which is a plausible assumption for dilute solutions. One could consider the situation when the particles disturb each other. These effects could be added into the theoretical description. In that respect, the region of the tube interior is the most critical since tubes can be very narrow and exclusion effects will be mostly pronounced in there.

In summary, the work we have presented is a step towards understanding the transport properties of large networks where geometrical concepts such as the length of the tubes play an important role. The setup employed in this study is rather simple. In order to be able to focus on issues related to transport, the reactions are totally omitted. The concentration profile in containers is assumed flat and this is good approximation when tubes are thin. A already simple examples of networks we studied show a number of interesting properties. For ex-

ample, transport properties of the networks exhibit large sensitivity to the geometrical changes in the structure. Also, one can adjust structure to obtain wave-like behavior (with one or two extremum points) in the curves that depict number of particles in containers. When the complexity of the network increases one can expect even more complicated behavior with larger number of extrema points. The setup we use is generic and it is possible to expand the model in many ways, e.g. by improving description of intra-container dynamics, incorporating reactions, or allowing particles to disturb each other. It will be an interesting problem to try to explore these questions further.

Acknowledgments

We would like to thank Prof. Owe Orwar and Prof. Mats Jonson for fruitful discussions.

APPENDIX A: NUMERICAL CONSIDERATIONS

In this section the numerical solution of Eq. (3) is discussed. In Section III and Section IV it was shown that the time derivatives $N_1(t); \dots; N_M(t)$ can be infinite at $t = 0$ which may cause numerical difficulties. However, the singular part of the derivative can be factored out by making the substitution

$$N_i(t) = (t)^{1=2} \tilde{N}_i(t); \quad i = 1; \dots; M \quad (A1)$$

where $\tilde{N}_i(t)$ is a smooth function of time. For small t the particles in the containers do not (yet) 'feel' the presence of another side and behave as if entering an infinitely long tube. An expression describing the transport behavior for such a case was found analytically and is stated in Eq. (20). The time derivative of Eq. (20) is proportional to $t^{1=2}$ for small t . Inserting Eq. (A1) in Eq. (3) yields an equation for $\tilde{N}_i(t)$ that was used for numerical calculations

$$\begin{aligned} \dot{\tilde{N}}_i(t) = & \sum_{j=1}^M C_{ji} \frac{V_{d-1}(a_{ji})}{V_d(R_j)} \frac{h}{t} R_t \frac{d}{dt} \tilde{N}_j(t) - \tilde{N}_i(t) \frac{h}{t} R_t \frac{d}{dt} \tilde{N}_i(t) \\ & + \sum_{j=1}^M \tilde{N}_j(0) \tilde{N}_j(t) \\ & + \sum_{j=1}^M C_{ij} \frac{V_{d-1}(a_{ij})}{V_d(R_i)} \frac{h}{t} R_t \frac{d}{dt} \tilde{N}_i(t) - \tilde{N}_i(t) \frac{h}{t} R_t \frac{d}{dt} \tilde{N}_i(t) \\ & + \frac{P}{D_{ij} t} R_t \frac{d}{dt} \tilde{N}_i(t) \\ & + \sum_{j=1}^M \tilde{N}_i(0) (\tilde{N}_{ij}(t) + \tilde{N}_{ji}(t)) : \end{aligned} \quad (A2)$$

Note that the expression for $\tilde{N}_{ij}(t)$ has been inserted into the integrals. Combining Eq. (20) and (A1) leads to

$$\tilde{N}_i(t) = N_{i0} (t)^{1=2} \tilde{N}_i(t); \quad i = 1; \dots; M : \quad (A3)$$

and sets the initial condition $\tilde{N}_i(0) = N_{i0}$.

From Eq. (A2) two types of integrals can be identified:

$$\begin{aligned} I_1^{t_n} [] &= \int_0^{t_n} \frac{dt}{(t_n - t)} (t) \\ I_2^{t_n} [] &= \int_0^{t_n} \frac{dt}{t} (t) \end{aligned} \quad (A4)$$

where (t) is non-singular in the range of integration. The quadrature formulas derived to solve $I_1^{t_n} []$ and $I_2^{t_n} []$ are based on the methods described in [37]. The idea is that the singular part of the integrand, $t^{1=2}$ and $[t(t_n - t)]^{1=2}$ respectively, is treated exactly while the smooth part $\tilde{N}_i(t)$ is linearly interpolated between t_i and t_{i+1} . The resulting quadrature formulas are of the form

$$I_1^{t_n} [] = \sum_{j=0}^{X^n} w_{nj} (t_j) \quad i = 1; 2 \quad (A5)$$

where w_{nj} are weights, $n = 1; 2; \dots$ and $t_n = nh$. This quadrature formula becomes exact when (t) is piecewise linear. Calculating weights for $I_1^n []$ yields

$$\begin{aligned} w_{n0} &= \frac{P}{n-1} (n-2) \arcsin \frac{1}{n} \\ w_{ij} &= \frac{P}{(j-1)(n-j+1)} + \frac{P}{(j+1)(n-j-1)} \\ &\quad - \frac{P}{2} \frac{j(n-j)+2j+1}{j(n-j)+2j+1} \arcsin \frac{j-1}{n} \\ &\quad - 2 \arcsin \frac{j}{n} + \arcsin \frac{j+1}{n} \\ w_{nn} &= \frac{P}{n-1} + \frac{1}{n} + (n-2) \arctan \frac{P}{n-1} : \end{aligned} \quad (A6)$$

Calculating weights for $I_2^n []$ yields

$$\begin{aligned} w_{n0} &= \frac{4h^{1=2}}{3} \\ w_{nj} &= \frac{4h^{1=2}}{3} (j+1)^{3=2} - 2j^{3=2} + (j-1)^{3=2} \\ w_{nn} &= \frac{2h^{1=2}}{3} n^{3=2} - 3(n-1)^{3=2} + 2(n-1)^{3=2} : \end{aligned} \quad (A7)$$

Finally, an expression for the total number of particles is found by integrating Eq. (A1)

$$N_i(t) = N_i(0) + \int_0^t \frac{dt}{t} \tilde{N}_i(t); \quad i = 1; \dots; M : \quad (A8)$$

$N_i(t); \dots; N_M(t)$ are found by using the quadrature formula derived for $I_2^n []$.

APPENDIX B: FINDING A SET OF APPROXIMATIVE RATE EQUATIONS FROM AN EXPANSION OF EQ. (39) IN THE VARIABLES.

In this section, details for obtaining a set of first order rate equations from Eq. (39) will be outlined. The dynamical equations are found by approximating M given

in Eq. (41). M is approximated by using the expansion stated in Eq. (53). The inverse Laplace transform of Eq. (39) after approximation reads

$$N_1(t) = \frac{3V_d(R_1)V_{tube}}{3V_d(R_1) + V_{tube}} \frac{D}{V_d(R_2)} \frac{N_2(t)}{V_d(R_1)} \frac{N_1(t)}{V_d(R_1)} \quad (B1a)$$

$$N_2(t) = \frac{3V_d(R_2)V_{tube}}{3V_d(R_2) + V_{tube}} \frac{D}{V_d(R_1)} \frac{N_1(t)}{V_d(R_1)} \frac{N_2(t)}{V_d(R_2)} \quad (B1b)$$

The decay rate predicted by these equations is given by $\frac{1}{\tau_{1,2}^0} = \frac{2}{\tau_{1,2}^0} D$ where

$$\frac{2}{\tau_{1,2}^0} = \frac{V_{tube}[V_d(R_1) + V_d(R_2)]}{V_d(R_2)[V_d(R_1) + V_{tube}=3]} \quad (B2)$$

This decay exponent is not adequate. For example, in the case where all volumes are equal $\frac{2}{\tau_{1,2}^0} = 1.5$ while the exact value is $\frac{2}{\tau_{1,2}^0} = 1.71$.

The rate Eq. (B1) can not describe the behavior of $N_{1,2}(t)$ as $t \rightarrow 1$ and $t \rightarrow 0$: the values for $N_{1,2}(1)$ are given by

$$\frac{N_1(1)}{V_d(R_1)} = \frac{N_2(1)}{V_d(R_1)} = \frac{N_{10} + N_{20}}{V_d(R_1) + V_d(R_2) + \frac{2}{3}V_{tube}} \quad (B3)$$

and for $N_{1,2}(0^+)$ there is a sudden jump

$$N_i(0^+) = \frac{N_{i0}}{1 + V_{tube}=3V_d(R_i)}; \quad i = 1, 2 \quad (B4)$$

and $N_i(0^+) \neq N_i(0)$. This is not satisfactory and another type of expansion is needed if correct limits and better decay rates are to be found.

APPENDIX C: RATE EQUATIONS FOR THE CASE STUDIES

This appendix explains in a more detail how to derive the rate equations used in the cases studies in Section V III. The equations are obtained from Eq. (3). Also, Eq. (59) is used to illustrate the impacts on dynamics from changes in the network structure in a less complicated form. The $N_i(t)$, $\dot{N}_{ij}(t)$, $\dot{N}_{ij}(t)$ and $\dot{N}_{ij}(t)$ are defined in Section II. The initial distribution is set to be $N_j(0) = N_{j0}$ where $j = 1; \dots; M$ and M is the total number of nodes in the system. Note the symmetry relations $a_{ij} = a_{ji}$, $\dot{N}_{ij} = \dot{N}_{ji}$ and $D_{ij} = D_{ji}$ which implies that $\dot{N}_{ij}(t) = \dot{N}_{ji}(t)$, $\dot{N}_{ij}(t) = \dot{N}_{ji}(t)$ and $\dot{N}_{ij}(t) = \dot{N}_{ji}(t)$ (see Eq. 5).

1. The Line

The structure of the linear network studied here is shown in Fig. 9 (a). Containers C_1 and C_3 are connected only to the middle container C_2 . Therefore, the

rate equations describing the dynamics in each container, $N_1(t)$ and $N_3(t)$ respectively, have the similar form :

$$N_1(t) = \frac{V_{d-1}(a_{21})}{V_d(R_2)} \frac{R_t}{0} dt N_2(t^0)_{21}(t-t^0) \quad (C1)$$

$$+ \frac{V_{d-1}(a_{12})}{V_d(R_1)} \frac{R_t}{0} dt N_1(t^0)_{12}(t-t^0) + \dots; \quad i = 1, 3:$$

The middle container C_2 is connected both to container C_1 and C_3 . The rate equations for $N_2(t)$ reads

$$N_2(t) = \frac{V_{d-1}(a_{12})}{V_d(R_1)} \frac{R_t}{0} dt N_1(t^0)_{12}(t-t^0) + \frac{V_{d-1}(a_{32})}{V_d(R_3)} \frac{R_t}{0} dt N_3(t^0)_{32}(t-t^0) + \frac{V_{d-1}(a_{21})}{V_d(R_2)} \frac{R_t}{0} dt N_2(t^0)_{21}(t-t^0) + \frac{V_{d-1}(a_{23})}{V_d(R_2)} \frac{R_t}{0} dt N_2(t^0)_{23}(t-t^0): \quad (C2)$$

Equations (C1) and (C2) have a quite complicated structure and impacts on the dynamics of $N_1(t)$, $N_2(t)$ and $N_3(t)$ due to changes in the structure (e.g tube lengths and container volumes) are not easily predicted. Simpler expressions can be obtained by using Eq. (59) which is valid in the large time limit under the assumption that the number of particles in the tubes is negligible over time. Applying Eq. (59) leads to

$$N_1(t) = \frac{V_{d-1}(a_{21})}{V_d(R_2)} \frac{D}{\tau_{21}} N_2(t) \quad (C3)$$

$$\frac{V_{d-1}(a_{12})}{V_d(R_1)} \frac{D}{\tau_{12}} N_1(t); \quad i = 1, 3$$

$$N_2(t) = \frac{V_{d-1}(a_{12})}{V_d(R_2)} \frac{D}{\tau_{12}} N_1(t) + \frac{V_{d-1}(a_{32})}{V_d(R_3)} \frac{D}{\tau_{32}} N_3(t) + \frac{D}{V_d(R_2)} \left(\frac{V_{d-1}(a_{12})}{\tau_{12}} + \frac{V_{d-1}(a_{23})}{\tau_{23}} \right) N_2(t):$$

2. The triangle

The triangular network studied here is depicted in Fig. 9 (b). All the containers C_1 , C_2 and C_3 are connected to each other and therefore the rate equations describing the time evolution of $N_1(t)$, $N_2(t)$ and $N_3(t)$ have the same form. Equation (C4) is the rate equation that governs the dynamics in container C_1 . The corresponding dynamical equations for $N_2(t)$ and $N_3(t)$ are obtained in the same way but are not written down here

APPENDIX D : ELIMINATION OF JUNCTIONS IN THE ASYMPTOTIC REGIME

$$\begin{aligned}
 N_1(t) = & \frac{V_{d-1}(a_{21})}{V_d(R_2)} R_t \int_0^t dt N_2(t^0)_{21}(t-t^0) \\
 & + \frac{V_{d-1}(a_{31})}{V_d(R_3)} R_t \int_0^t dt N_3(t^0)_{31}(t-t^0) \\
 & + \frac{V_{d-1}(a_{12})}{V_d(R_1)} R_t \int_0^t dt N_1(t^0)_{12}(t-t^0) + \frac{V_{d-1}(a_{13})}{V_d(R_1)} R_t \int_0^t dt N_1(t^0)_{13}(t-t^0) \quad (C4)
 \end{aligned}$$

The behavior of $N_1(t)$, $N_2(t)$ and $N_3(t)$ are very sensitive to changes in the network structure. The response from these changes are not easily predicted by Eq. (C4). Instead Eq. (59) can be used to state a simplified version of Eq. (C4). Note that this equation only is valid in the large time limit if the number of particles in the tubes is small. Applying Eq. (59) to container C_1 in the triangular network gives

$$\begin{aligned}
 N_1(t) = & \frac{V_{d-1}(a_{21})}{V_d(R_2)} \frac{D}{V_{21}} N_2(t) + \frac{V_{d-1}(a_{31})}{V_d(R_3)} \frac{D}{V_{31}} N_3(t) \\
 & + \frac{D}{V_d(R_1)} \left[\frac{V_{d-1}(a_{12})}{V_{12}} + \frac{V_{d-1}(a_{13})}{V_{13}} \right] N_1(t) \quad (C5)
 \end{aligned}$$

Corresponding first order rate equations for $N_2(t)$ and $N_3(t)$ are found in the same way.

3. The T-Network

The T-shaped network under investigation in this subsection is depicted in Fig. 9 (c). Since all containers C_1 , C_2 and C_3 are connected to container C_4 and not to each other, the rate equations governing the dynamics in C_1 , C_2 and C_3 , that is $N_1(t)$, $N_2(t)$ and $N_3(t)$ respectively, all have similar form,

$$\begin{aligned}
 N_i(t) = & \frac{V_{d-1}(a_{i4})}{V_d(R_4)} R_t \int_0^t dt N_4(t^0)_{4i}(t-t^0) \\
 & + \frac{V_{d-1}(a_{i4})}{V_d(R_i)} R_t \int_0^t dt N_i(t^0)_{i4}(t-t^0) \quad (C6) \\
 & + \frac{V_{d-1}(a_{i4})}{V_d(R_i)} R_t \int_0^t dt N_i(t^0)_{i4}(t-t^0); \quad i = 1; 2; 3:
 \end{aligned}$$

The middle container C_4 has connections to all other containers C_1 , C_2 and C_3 . This leads to a rate equation for $N_4(t)$ on the form

$$\begin{aligned}
 N_4(t) = & \sum_{j=1}^3 \frac{V_{d-1}(a_{j4})}{V_d(R_j)} R_t \int_0^t dt N_j(t^0)_{j4}(t-t^0) \\
 & + \frac{1}{V_d(R_4)} R_t \int_0^t dt N_4(t^0) \\
 & + \sum_{j=1}^3 V_d(a_{4j}) [N_4(t-t^0)_{4j} + N_4(t-t^0)_{j4}] \quad (C7)
 \end{aligned}$$

The rate equations derived in this subsection are used in the study of the junction, shown in Fig. 14.

The network studied in this section is a generalization of the one depicted in Fig. 14. Here, a junction having an arbitrary number of connections is studied and it will be demonstrated that the dynamical equations governing the transport in a system having junction points can be simplified in the large time limit. First, it will be shown that the current of particles in and out of a junction point eventually will balance each other out and that this occurs faster than the time it takes before an equilibrium particle distribution is attained throughout the network. This derives from the fact that the volume of the junction (proportional to a^d) is much smaller than the volumes of the containers, (proportional to R_i^d , $i = 1; \dots; M$), where d is the dimensionality, a is the tube radius and M is the number of containers. The tubes connecting the junction are assumed to have the same radius. Second, it will be demonstrated how to simplify the transport equations in such a way that the dynamical variable for the junction $N(t)$ can be eliminated completely. This might be desirable when working with large networks.

Consider a junction with dynamical behavior contained in $N_j(t)$ and volume $V_d(a)$ that has connections to M containers with volumes $V_d(R_i)$, $i = 1; \dots; M$. The equation governing the dynamics of the junction point written in Laplace space reads

$$\begin{aligned}
 sN_j(s) - N_j(0) = & -sN_j(s) \frac{V_{d-1}(a)}{V_d(a)} \sum_{i=1}^M [j_i(s) + j_i(s)] \\
 & + \sum_{i=1}^M sN_i(s) \frac{V_{d-1}(a)}{V_d(R_i)} i_j(s) \quad (D1)
 \end{aligned}$$

This equation is a generalization of Eqs. (29) (see Section VI). The junction point studied here is such that $a = R_i$ and since

$$\frac{V_{d-1}(a)}{V_d(a)} = C_d \frac{1}{a}; \quad \frac{V_{d-1}(a)}{V_d(R_i)} = C_d \frac{1}{a} \frac{a^d}{R_i^d} \quad (D2)$$

where $C_d = \frac{d}{d-1} \left[\frac{d-1}{2} \right]^{1-d/2}$ [found by using the formula for a d -dimensional sphere, see Section II] the term proportional to $(a/R_i)^d$ can be neglected and a closed expression for $N_j(s)$ can be obtained. Solving Eq. (D1) after eliminating the second term leads to

$$N_j(s) = \frac{N_j(0)}{s + 1 + \frac{C_d}{a} \sum_{i=1}^M [j_i(s) + j_i(s)]} \quad (D3)$$

The inverse Laplace transform of $N_j(s)$ is a sum of exponentials

$$N_j(t) = \sum_{p=1}^X p e^{-p t} \quad (D4)$$

where p is the residue of $N_j(s)$ at pole $s = -p$,

$p < 0$. The poles are given by the zeros of

$$s + \sum_{i=1}^M C_{ij} \frac{q_{ij} D_{ij} \cosh q_{ij}}{a_{ij} \sinh q_{ij}} = 0 \quad (D 5)$$

where $q_{ij}^2 = s_{ij}^2 D_{ij}$. When the currents in and out of the junction point balances each other out there is no accumulation of particles and $N_j(t) = 0$. This is easily verified from Eq. (D 4) by evaluating the derivative in respect to t at $t = 1$

$$\frac{d}{dt} N_j(t) = \sum_{p=1}^M (-p) p e^{-pt} \neq 0 \text{ as } t \rightarrow 1 : \quad (D 6)$$

Let τ_{junction} be an estimate of the time it takes until $N_j(t) = 0$. It is related to the decay exponents p (see Eqs. 38 and 43) which are zeros of Eq. (D 5). From Eq. (D 5) it is clear that the zeros scales with $\frac{D}{a}$ (it is assumed that $D_{ij} = D$ and $a_{ij} = a$) which leads to the estimate $\tau_{\text{junction}} \propto \frac{a}{D}$. Let τ_{network} be an estimate of the time it takes to reach an overall equilibrium particle distribution in the network. As a rough estimate Eq. (50) can be used which was found for a two-node network. If the containers have volumes proportional to R^d then $\tau_{\text{network}} \propto \frac{a}{D} \frac{R^d}{a}$. If $R \propto a$ then $\tau_{\text{junction}} \propto \tau_{\text{network}}$. This is supported by the numerical calculation shown in Fig. 15 where the curve corresponding to $N_4(t)$ attains out relatively fast.

For networks where there are many junctions and containers involved it might be desirable to reduce the number of variables in the dynamical equations governing the particle transport. This can be done in the regime where $N_j(t) = 0$ is valid and Eq. (59) is applicable. Applying

Eq. (59) for a junction point j having M connections and using $N_j(t) = 0$ leads to

$$0 = \sum_{i=1}^M C_{ij} V_{d-1}(a) \frac{D_{ij}}{a_{ij}} \frac{N_i(t)}{V_d(R_i)} \frac{N_j(t)}{V_d(a)} \quad (D 7)$$

In this way it is possible to express $N_j(t)$ in terms of $N_1(t); \dots; N_M(t)$. Inserting the solution to this matrix equation in the dynamical equations eliminates the explicit dependence of $N_j(t)$. Eqs. (D 8) – (D 10) shows this explicitly for the case of a three way junction depicted in Fig. 14, where $N_4(t)$ has been taken away completely

$$N_1(t) = \frac{\frac{1}{2} D \frac{V_{d-1}(a)}{V_d(R_2)}}{\frac{1}{2} D \frac{V_{d-1}(a)}{V_d(R_1)}} N_2(t) + \frac{\frac{1}{2} D \frac{V_{d-1}(a)}{V_d(R_3)}}{\frac{1}{2} D \frac{V_{d-1}(a)}{V_d(R_1)}} N_3(t) \quad (D 8)$$

$$\frac{(\frac{1}{2} + \frac{1}{2}) D \frac{V_{d-1}(a)}{V_d(R_1)}}{\frac{1}{2} D \frac{V_{d-1}(a)}{V_d(R_1)}} N_1(t)$$

$$N_2(t) = \frac{\frac{1}{2} D \frac{V_{d-1}(a)}{V_d(R_1)}}{\frac{1}{2} D \frac{V_{d-1}(a)}{V_d(R_2)}} N_1(t) + \frac{\frac{1}{2} D \frac{V_{d-1}(a)}{V_d(R_3)}}{\frac{1}{2} D \frac{V_{d-1}(a)}{V_d(R_2)}} N_3(t) \quad (D 9)$$

$$\frac{(\frac{1}{2} + \frac{1}{2}) D \frac{V_{d-1}(a)}{V_d(R_2)}}{\frac{1}{2} D \frac{V_{d-1}(a)}{V_d(R_2)}} N_2(t)$$

$$N_3(t) = \frac{\frac{1}{2} D \frac{V_{d-1}(a)}{V_d(R_2)}}{\frac{1}{2} D \frac{V_{d-1}(a)}{V_d(R_3)}} N_1(t) + \frac{\frac{1}{2} D \frac{V_{d-1}(a)}{V_d(R_2)}}{\frac{1}{2} D \frac{V_{d-1}(a)}{V_d(R_3)}} N_2(t) \quad (D 10)$$

$$\frac{(\frac{1}{2} + \frac{1}{2}) D \frac{V_{d-1}(a)}{V_d(R_3)}}{\frac{1}{2} D \frac{V_{d-1}(a)}{V_d(R_3)}} N_3(t)$$

$$\frac{1}{2} \frac{1}{2} \frac{1}{2} + \frac{1}{2} \frac{1}{2} \frac{1}{2} + \frac{1}{2} \frac{1}{2} \frac{1}{2} :$$

-
- [1] R. Albert and A.L. Barabasi, Rev. Mod. Phys. 74, 47-94 (2002).
- [2] P. Stange, D. Zanette, A. Mikhailov and B. Hess, Biophys. Chem. 79, 233-247 (1999).
- [3] P.L. Krapivsky, S. Redner, and F. Leyvraz, Phys. Rev. Lett. 85, 4629 (2000).
- [4] F. Slanina and M. Kotrla, Phys. Rev. Lett. 83, 5587 (1999).
- [5] D.J. Watts, Small Worlds: The Dynamics of Networks between Order and Randomness, (Princeton University, Princeton, NJ), 1999.
- [6] S. Jain and S.K. Krishna, Phys. Rev. Lett. 81, 5684 (1998).
- [7] A. Karlsson, R. Karlsson, M. Karlsson, F. Ryttsen and O. Rowar, Nature 409, 150-153 (2001).
- [8] I.V. Grigoriev, Y.A. Makhnovskii, A.M. Berezhkovskii, V.Y. Zitserman, J. Chem. Phys. 116, 9574 (2002).
- [9] A.M. Berezhkovskii and A.V. Barzykin, Chem. Phys. Lett. 383, 6-10 (2004).
- [10] L. Dagdug, A.M. Berezhkovskii, S.Y. Shvartsman, G.H. Weiss, J. Chem. Phys. 119, 12473 (2003).
- [11] L. Dagdug, A.M. Berezhkovskii and G.H. Weiss, Phys. Rev. E 69, 012902 (2004).
- [12] S.M. Bezukov, A.M. Berezhkovskii, M.A. Pustovit, A. Szabo, J. Chem. Phys. 113, 8206-8211 (2000).
- [13] D.J. Watts and S.H. Strogatz, Nature 393, 440-442 (1998).
- [14] M.L. Simpson, G.S. Saylor, J.T. Fleming and B. Applegate, Trends in Biotechnology 19(8), 317 (2001).
- [15] V.K. Krishnamurthy and E.V. Krishnamurthy, BioSystems 49, 205 (1999).
- [16] N.G. Rambidi, BioSystems 44, 1-15 (1997).
- [17] M. Conrad and K.P. Zauner, BioSystems 45, 59 (1998).
- [18] K.P. Zauner and M. Conrad, Soft Computing 5, 39 (2001).
- [19] K.P. Zauner and M. Conrad, Naturwissenschaften 87, 360 (2000).
- [20] S. Ji, BioSystems 52, 123 (1999).
- [21] C. Siehs and B. Mayer, Nanotechnology 10, 464 (1999).
- [22] J.P. Laplante, M. Pemberton, A.H. Jelmfelt and J. Ross, J. Phys. Chem. 99 (25), 10063 (1995).
- [23] A.H. Jelmfelt and J. Ross, J. Phys. Chem. 97, 7988 (1993).
- [24] A.H. Jelmfelt, F.W. Schneider and J. Ross, Science 260, 335 (1993).
- [25] K. Akingbehin, BioSystems 35, 223 (1995).
- [26] K. Akingbehin and M. Conrad, Journal of Parallel and Distributed Computing 6, 245 (1989).
- [27] M. Conrad, European Journal of Operational Research 30, 280 (1987).

- [28] K.G. Kirby and M. Conrad, *Physica D* 22, 205 (1986).
- [29] K.G. Kirby and M. Conrad, *Bulletin of Mathematical Biology* 46 (5/6), 765 (1984).
- [30] R. Kampfer and M. Conrad, *Bulletin of Mathematical Biology* 45 (6), 931 (1983).
- [31] R. Kampfer and M. Conrad, *Bulletin of Mathematical Biology* 45 (6), 969 (1983).
- [32] H.C. Berg and E.M. Purcell, *BioPhys. J.* 20, 193 (1977).
- [33] M.A. Spiegel, *Schaum's outline of Laplace Transforms*, Cambridge University Press (1986).
- [34] W.R. LePage, *Complex variables and the Laplace Transform for engineers*, Dover Publications Inc., New York (1980).
- [35] W.H. Press, B.P. Flannery, A.S. Teukolsky and W.T. Vetterling, *Numerical Recipes*, Cambridge University Press, New York (1986).
- [36] A.H. Jelmfelt, F.W. Schneider, *J. Ross. Science* 260, 335-337 (1993).
- [37] L.M. Delves, J.L. McMahon, *Computational Methods for integral equations*, Cambridge University Press, London (1985).
- [38] An alls expansion of Eq. (23) and (31) in Laplace transform space yields $L^{-1}[(s)]/t^{1/2}$ and $L^{-1}[(s)]/\text{const.}$ Since (t) and (t) always combine in a sum, (t) will dominate the output for large t .
- [39] τ_{target} is derived under the assumption of a fully absorbing target of radius a . This is not a correct description of a tube opening since it allows reentry. This estimate serves however as a worst case scenario.

FIGURES

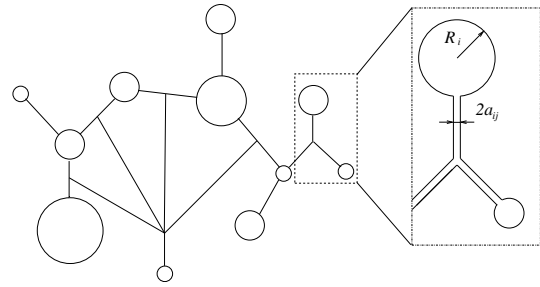


FIG. 1: Schematic picture of an arbitrary network built from containers and tubes.

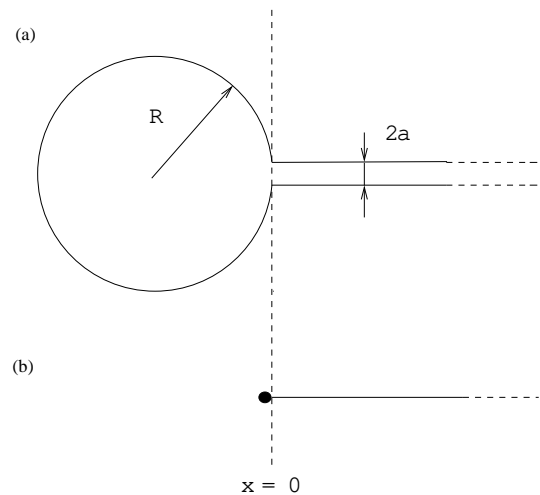


FIG. 2: Panel (a): A spherical compartment connected to a cylindrical infinitely long tube. If the tube radius is assumed to be small the compartment can be treated as ideally mixed at all times simplifying the dynamics in the container. The transport in the tube is reduced to a one dimensional diffusion problem. Panel (b) illustrates these simplifications.

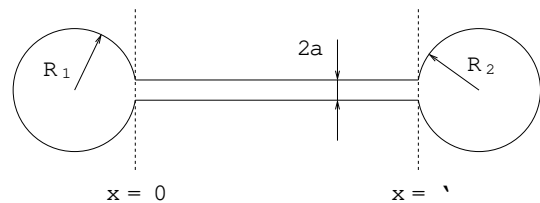


FIG. 3: Schematic picture of a two-node network.

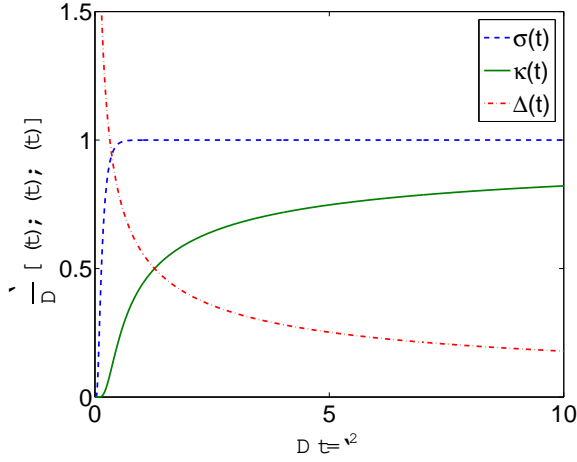


FIG. 4: Time dependence of the rate coefficients $\sigma(t)$, $\kappa(t)$ and $\Delta(t)$ from Eq. (3).

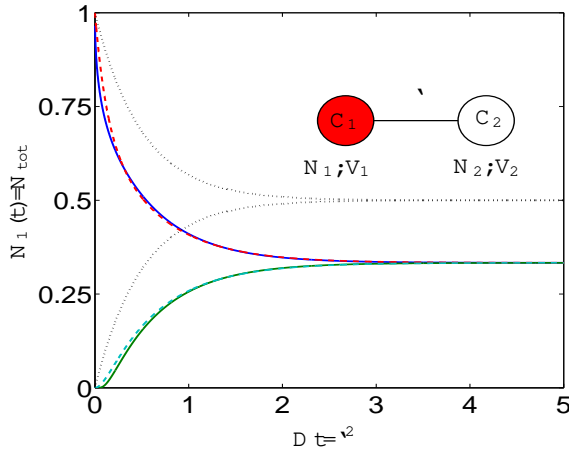


FIG. 5: The solution of Eq. (35) (solid line) is compared with a solution of Eq. (55) (dashed line). The solution of Eq. (45), given in (49), is represented by the dotted line. The curves decaying and growing describe $N_1(t)$ and $N_2(t)$ respectively. The network structure is shown in inset. The volumes of the tube and the containers are equal and $a=v=0.05$. The initial distribution of particles is $N_1(0)=N_{\text{tot}}=1$ and $N_2(0)=0$, where $N_{\text{tot}}=N_1(0)+N_2(0)$, indicated by the shading in inset. This figure clearly shows that Eq. (49) does not lead to the correct values for $N_1(t)$ and $N_2(t)$. The agreement with Eq. (55) is much better.

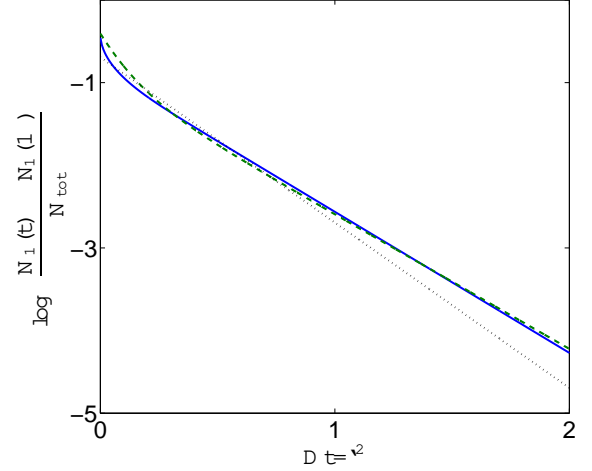


FIG. 6: The natural logarithm of $N_1(t) - N_1(1)/N_{\text{tot}}$ for the three cases illustrated in Fig. 5. The labeling of the curves is the same as in Fig. 5. The linear behavior is the evidence of the single exponential decay of the number of particles in the container C_1 . The slope gives the value of the decay exponent. The slopes of the solid and dashed lines are close to each other showing that Eq. (55) is capable of estimating the decay exponent well. The slope of the dotted line differs significantly from the others which illustrates that Eq. (49) can not describe the dynamics in an adequate way. Since the value of $N_1(1)$ is not the same as in all three cases [compare Eq. (51) and (52)] the value of $N_1(0) - N_1(1)$ will be different. This explains why all three curves do not coincide at $t=0$.

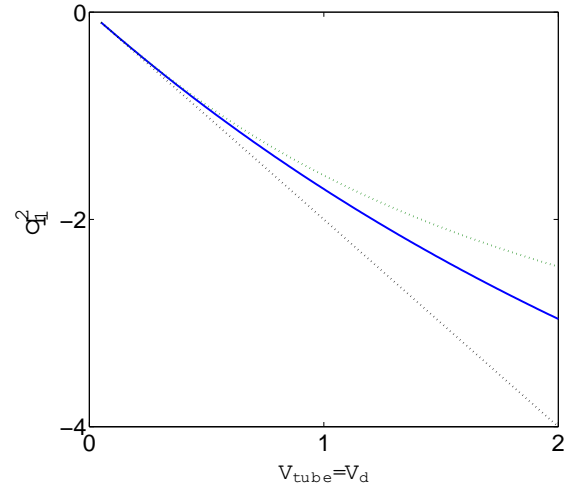


FIG. 7: Dependence of the geometrical factor q^2 on the tube volume. (The volumes of the containers are equal $V_d(R_1) = V_d(R_2) = V_d$.) q^2 and V_d are related through $V_d = q^2 D \tau^2$. The numerical solution of Eq. (42), which gives the exact values for q^2 , is represented by the solid line. It is compared with the values for q^2_{ja} (Eq. 50), dashed line, and q^2_{jb} (Eq. 56), dotted line. The dotted line deviates significantly from the solid one as $V_{tube}=V_d$ increases while the dashed line follows the exact solution better. This indicates that q^2_{jb} provides a good estimate of the decay rate, even for large tube volumes. q^2_{ja} can only be used for very small values of $V_{tube}=V_d$.

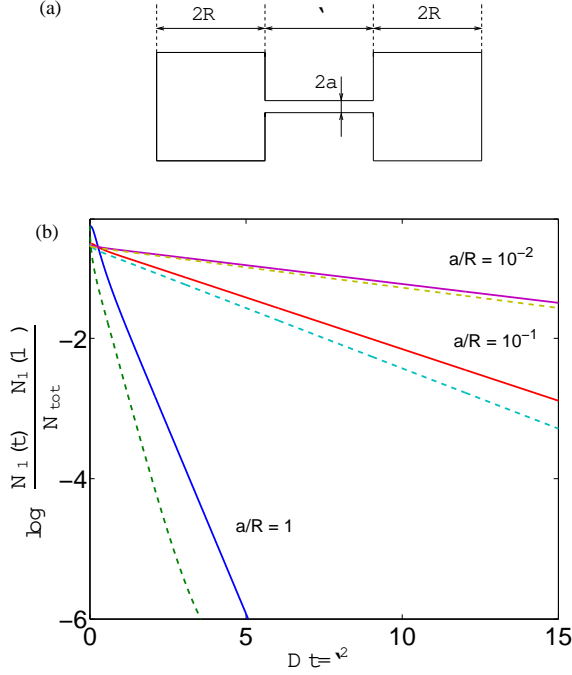


FIG. 8: A numerical verification of the assumption of well stirred containers. For simplicity reasons a cubic geometry, as depicted in panel (a), was chosen since the explicit shape of the container loses its importance for large reservoir volumes. The edge length is set to $2R$ where R is the radius of an equivalent spherical container. Panel (b) shows a numerical solution to the 2D-diffusion equation (solid line) compared to a numerical solution to Eqs. (3) (dashed line). The cases are chosen so that $a=R$ varies in three orders of magnitude showing increasing validity of the assumption of ideally mixed containers as $a=R$ decreases. The initial distribution in all three cases are skewed (a delta function in the bottom right corner of the left container) which becomes important when a is large. For small a , τ_{mix} is a lot shorter than τ_{target} and the skewed initial distribution will have time to smear out before particles start exiting and the shape of the initial distribution has no effect.

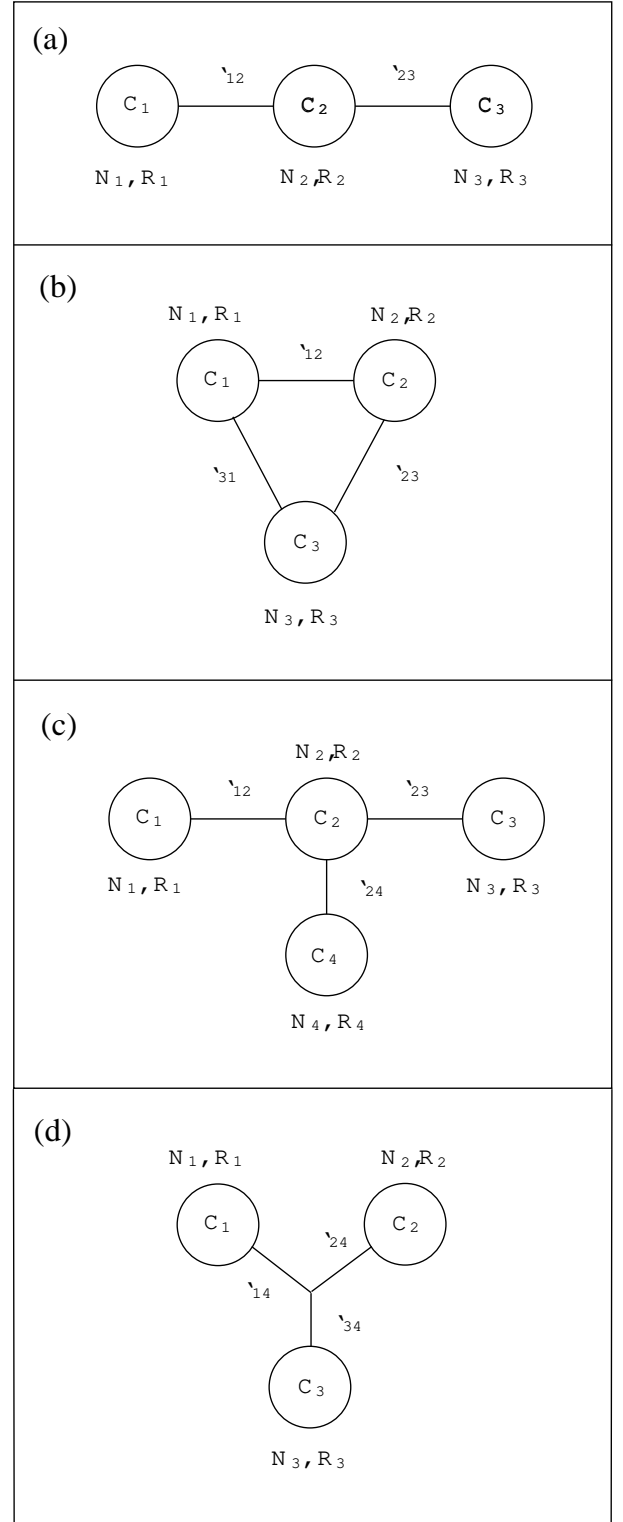


FIG. 9: networks used for case studies in Section VIII. Panels (a)-(d) corresponds to cases 1-4.

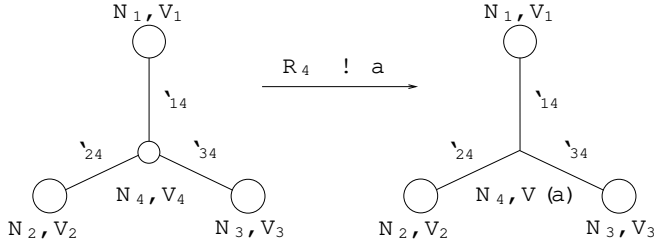


FIG. 14: The transformation from a four-node network to a network involving a three way junction.

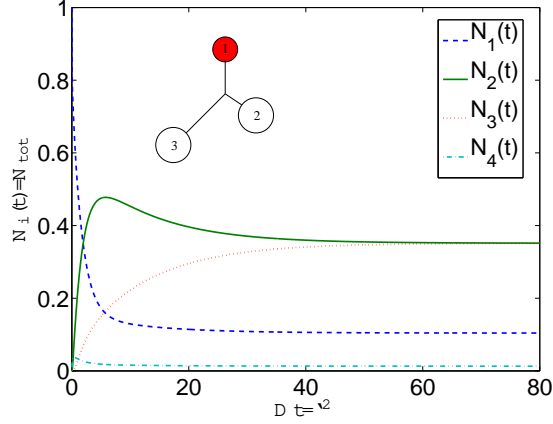


FIG. 15: The transport properties for the network involving a three way junction shown in Fig. 9 (d), see Section V III (case 4) for discussion. The curves depict a numerical solution of Eqs. (C 6) and (C 7) [with $V_d(R_4) = V_d(a)$]. The system parameters were set to $\lambda_{12}=a = 2$, $\lambda_{13}=a = 10$, $\lambda_{14}=a = 20$, $R_1=a = 2$ and $R_2=a = R_3=a = 4$. Initial distribution of particles $N_1(0)=N_{\text{tot}} = 1$, $N_2(0)=N_{\text{tot}} = N_3(0)=N_{\text{tot}} = N_4(0)=N_{\text{tot}} = 0$ is shown in inset.

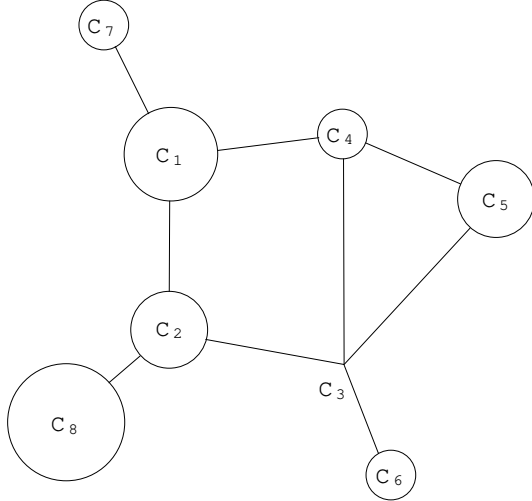


FIG. 16: Structure of the network studied in Section V III, case 5. The parameters describing the geometry are labeled in the same way as in Fig. 9. The parameters used were $a=\lambda_{12}=3$, $\lambda_{23}=\lambda_{13}=1$, $\lambda_{45}=\lambda_{14}=9$, $\lambda_{43}=\lambda_{10}=10$, $\lambda_{35}=\lambda_{8}=8$, $\lambda_{36}=\lambda_{2}=2$, $\lambda_{28}=\lambda_{01}=0.1$, $\lambda_{12}=\lambda_{1}=1$, $\lambda_{32}=\lambda_{1}=1$, $R_1=a = 4$, $R_2=a = 2$, $R_3=a = 1$, $R_4=a = 2.5$, $R_5=a = 3$, $R_6=a = 2$, $R_7=a = 2$, $R_8=a = 4$.

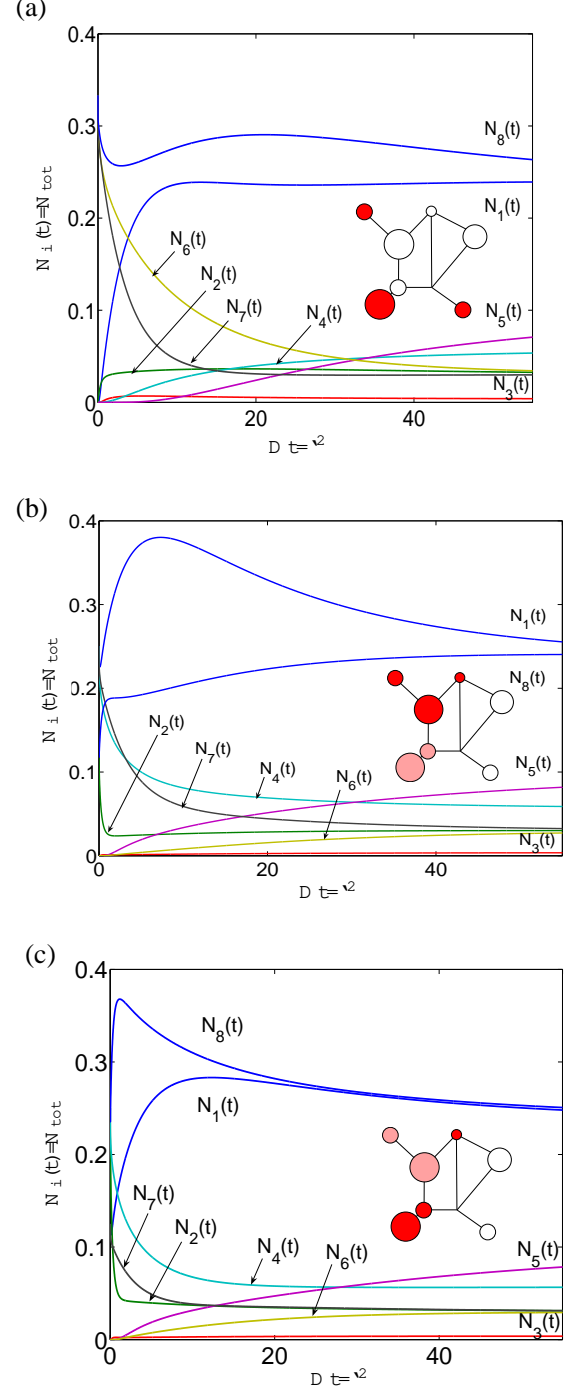


FIG. 17: The solution of Eq. (3) for the network depicted in Fig. 16. The panel includes graphs showing the transport dynamics for three different choices of initial distribution of particles. Panel (a): $N_1(0) = N_2(0) = N_3(0) = N_4(0) = N_5(0) = 0$, $N_6(0) = N_7(0) = N_8(0) = 1=3$; Panel (b): $N_3(0) = N_5(0) = N_6(0) = 0$, $N_2(0) = N_8(0) = 1=8$ and $N_1(0) = N_4(0) = N_7(0) = 1=4$; Panel (c): $N_3(0) = N_5(0) = N_6(0) = 0$, $N_1(0) = N_7(0) = 1=8$ and $N_2(0) = N_4(0) = N_8(0) = 1=4$ where $N_i(t) = N_i(t)/N_{\text{tot}}$, $i = 1; \dots; 8$. The initial conditions are also illustrated in the insets: a darker shading indicates that more particles are injected into the container.